Fac-to-*mer* isomerization triggers hydride transfer from Mn(I) complex *fac*-[$(Ph_2PCH_2PPh_2)Mn(CO)_3H$]

Elena S. Osipova,[a]† Ekaterina S. Gulyaeva,[a,b]† Nikolay V. Kireev,[a] Sergey A. Kovalenko,[a] Christian Bijani,[b] Yves Canac,[b] Dmitry A. Valyaev,*[b] Oleg A. Filippov,*[a] Natalia V. Belkova[a] and Elena S. Shubina*[a]

a - A. N. Nesmeyanov Institute of Organoelement Compounds (INEOS), Russian Academy of Sciences, 28 Vavilov str., GSP-1, B-334, Moscow, 119991, Russia

E-mails: h-bond@ineos.ac.ru, shu@ineos.ac.ru

b - LCC-CNRS, Université de Toulouse, CNRS, 205 route de Narbonne 31077 Toulouse, Cedex 4, France. E-mail: dmitry.valyaev@lcc-toulouse.fr

Electronic Supplementary Information

Table of contents

General considerations and synthesis of Mn(I) hydride complexes.

All manipulations were performed using standard Schlenk techniques under an atmosphere of dry nitrogen or argon. Dry and oxygen-free organic solvents (toluene, CH_2Cl_2) used for synthesis were obtained using LabSolv (Innovative Technology) solvent purification system. Commercially available dry ethanol was degassed by nitrogen bubbling for 10 min and stored under 4 Å molecular sieves. CH_2Cl_2 and *n*BuCl used for IR spectroscopy studies were stored over CaH_2 and distilled under an argon atmosphere prior to use. Deuterated solvents for NMR were degassed before use by three freeze-pump-thaw cycles and kept over 3 Å molecular sieves. A liquid nitrogen/ethanol or isopropanol slush bath was used to maintain samples at the desired low temperature. Manganese hydride complexes *fac*-[(dppm)Mn(CO)$_3$H] (*fac*-**1**) and *fac*-[(dppmD$_2$)Mn(CO)$_3$D] (*fac*-**1**-*d*$_3$) were prepared from the corresponding bromide precursor *fac*-[(dppm)Mn(CO)$_3$Br][1] and $NaBH_4$ using the modified literature procedure.[2] Commercially available $B(C_6F_5)_3$ and $[Ph_3C](B(C_6F_5)_4)$ were purified by vacuum sublimation and recrystallization from CH_2Cl_2/hexane mixture, respectively. All other reagent grade chemicals purchased from commercial sources were used as received.

Routine ^{1}H, ^{31}P and ^{13}C NMR spectra were recorded on Bruker Avance 400 and Avance III HD 400 spectrometers at 400.1, 162.0 and 100.6 MHz, respectively. Low-temperature NMR experiments were carried out using Bruker Avance NEO 600 spectrometer in the 183–303 K temperature range. ^{1}H and ^{13}C signals reported in parts per million (ppm) were calibrated against the residual signals of the deuterated solvent,[3] whereas ^{31}P and ^{11}B NMR spectra were referenced to 85% H_3PO_4 and $BF_3{\times}OEt_2$, respectively. When required, signal attribution in ^{13}C spectra was based on decoupled $^{13}C\{^{31}P,^1H\}$ and $^{13}C–^1H$ HSQC experiments. Variable temperature (160–293 K) IR spectra were recorded on Nicolet 6700 spectrometer using a home-modified cryostat (Carl Zeiss Jena, the accuracy of temperature adjustment ±0.5 K) and 0.05 cm CaF_2 cells.

Modified procedure for the synthesis *fac*-[(Ph$_2$PCH$_2$PPh$_2$)Mn(CO)$_3$H] (*fac*-1). A solution of (dppm)Mn(CO)$_5$Br (1.1 g, 1.82 mmol) and $NaBH_4$ (345 mg, 9.12 mmol) in EtOH (30 mL) were heated at 80 °C during 1 h until the disappearance of ν_{CO} bands of the precursor (ν_{CO} 2020 (vs), 1950 (s), 1917 (s) cm^{-1}). The resulting suspension was cooled to room temperature and the volatiles were removed under vacuum. The product was extracted with toluene (3×15 mL) and combined extracts were filtered through Celite and evaporated under reduced pressure. The residue was dissolved in CH_2Cl_2 (10 mL), the solution was again filtered through Celite and hexane (60 mL) was added under stirring. The resulting suspension was concentrated to *ca.* 30% of the initial volume and the supernatant was removed by decantation. The precipitate was washed with hexane (2×20 mL) and dried under vacuum to afford *fac*-**1** (860 mg, 90%) as pale-yellow solid.

fac-**1**: ^{1}H NMR (400.1 MHz, 298 K, CD_2Cl_2): δ 7.70−7.65 (m, 4H, C*H*$_{Ar}$), 7.59−7.54 (m, 4H, C*H*$_{Ar}$), 7.43−7.41 (m, 12H, C*H*$_{Ar}$), 4.42 (dtd, $^2J_{HH}$ = 15.0 Hz, $^2J_{PH}$ = 9.4 Hz, $^4J_{HH}$ = 5.5 Hz, 1H, PC*H*$_2$P), 4.03 (dt, $^2J_{HH}$ = 15.2 Hz, $^2J_{PH}$ = 11.0 Hz, 1H, PC*H*$_2$P), −5.56 (td, $^2J_{PH}$ = 44.0 Hz, $^4J_{HH}$ = 5.5 Hz, 1H, Mn−*H*). $^{31}P\{^1H\}$ NMR (162.0 MHz, 298 K, CD_2Cl_2): δ 32.6 (br s). IR (CH_2Cl_2): ν_{CO} 1995, 1915, 1905 cm^{-1}. IR (*n*BuCl): ν_{CO} 1993, 1911, 1902 cm^{-1}. IR (toluene): ν_{CO}: 1996, 1916, 1909 cm^{-1}.

Synthesis *fac*-[(Ph$_2$PCD$_2$PPh$_2$)Mn(CO)$_3$D] (*fac*-1-*d*$_3$). A solution of (dppm)Mn(CO)$_5$Br (60 mg, 0.10 mmol) and $NaBH_4$ (21 mg, 0.50 mmol) in EtOD (2 mL) was heated at 80 °C during 30 min and then kept overnight at 50 °C. The resulting suspension was cooled to room temperature and the volatiles were removed under vacuum. The product was extracted with toluene (3×5 mL), combined extracts were filtered through Celiteand evaporated under reduced pressure. The residue was triturated with pentane (2×2 mL) and dried under vacuum to afford *fac*-**1**-***d*$_3$** (31 mg, 59%) as pale-yellow solid. According to ^{1}H NMR data hydride and PCH_2P positions had more than 94% of deuterium incorporation.

fac-**1**-*d*$_3$: ^{1}H NMR (400.1 MHz, C_6D_6, 298 K): δ 7.71−7.66 (m, 4H, C*H*$_{Ar}$), 7.46−7.41 (m, 4H, C*H*$_{Ar}$), 7.03−6.92 (m, 12*H*, CH$_{Ar}$). $^{31}P\{^1H\}$ NMR (162.0 MHz, C_6D_6, 298 K): δ 34.0 (s). $^{13}C\{^1H\}\{^{31}P\}$ NMR (100.6 MHz, C_6D_6, 298 K): δ 225.1 (br s, Mn–CO), 222.4 (br s, Mn–CO), 138.0, 135.8 (s, *C*$_{ipso}$ PPh$_2$), 132.1, 130.3, 130.2, 128.8 (s, *C*H$_{Ar}$), 48.0 (quint, $^1J_{CD}$ = 21.7 Hz, P*C*D$_2$P). IR (CH_2Cl_2): ν_{CO} 1993, 1911, 1899 cm^{-1}. IR (*n*BuCl): ν_{CO} 1995, 1915, 1904 cm^{-1}.

General procedure for variable temperature IR studies.

The solution (c = 0.003 M) of *fac*-[(dppm)Mn(CO)$_3$H] (*fac*-**1**, 1.3 mg) prepared at room temperature in 0.8 mL of the corresponding solvent (CH_2Cl_2, *n*BuCl, toluene) was cannulated under an inert atmosphere into the cryostat and cooled to 160 K or 180 K. After the acquisition of reference IR spectrum of initial complex, the solution was removed from the cryostat to the Schlenk tube and cooled to 160 K or 180 K in liquid nitrogen/*i*PrOH or EtOH slush bath. The corresponding Lewis acid ([Ph_3C][$B(C_6F_5)_4$]: 2.2 mg, 1 equiv.; $B(C_6F_5)_3$: 1.2-1.8 mg, 1-1.5 equiv.) dissolved in a small amount of solvent (0.05-0.1 mL) was then added at low temperature and the resulting mixture was quickly mixed and returned into the cryostat and monitored by IR spectroscopy in the 160–290 K temperature range.

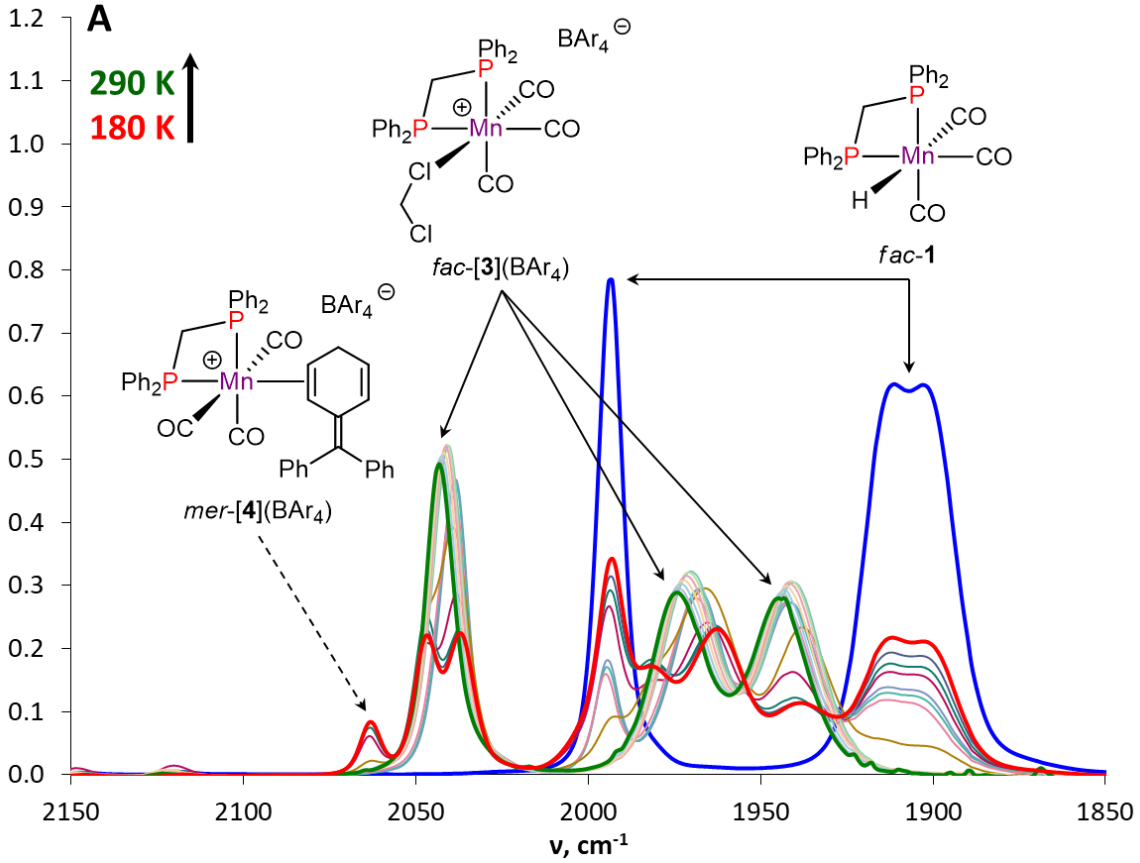

Figure S1. IR spectroscopy monitoring of the reaction of complex *fac*-**1** with 1 equiv. of [Ph_3C][BAr_4), Ar = C_6F_5) in CH_2Cl_2 at 180-300 K temperature range (c = 0.003 M, l = 0.05 cm).

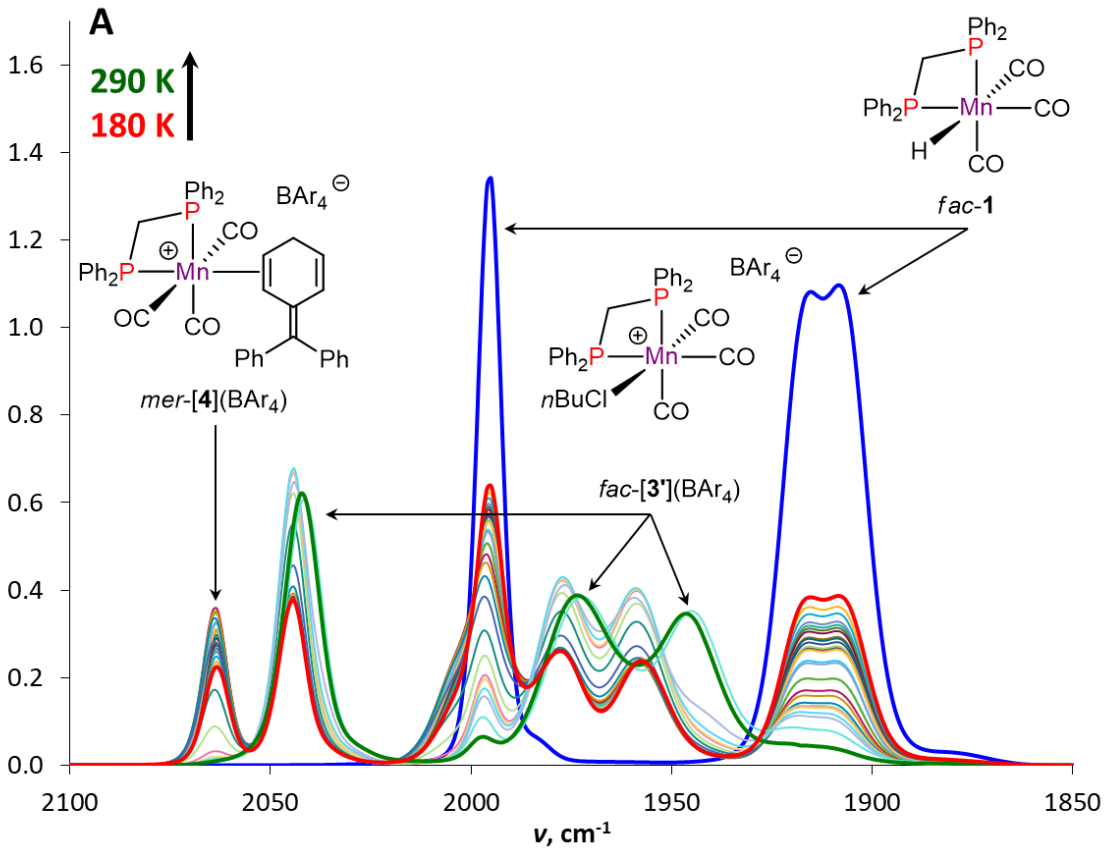

Figure S2. IR spectroscopy monitoring of the reaction of complex *fac*-**1** with 1 equiv. of $[Ph_3C](BAr_4)$ (Ar = C_6F_5) in *n*BuCl at 160-300 K temperature range (*c* = 0.004 M, *l* = 0.05 cm).

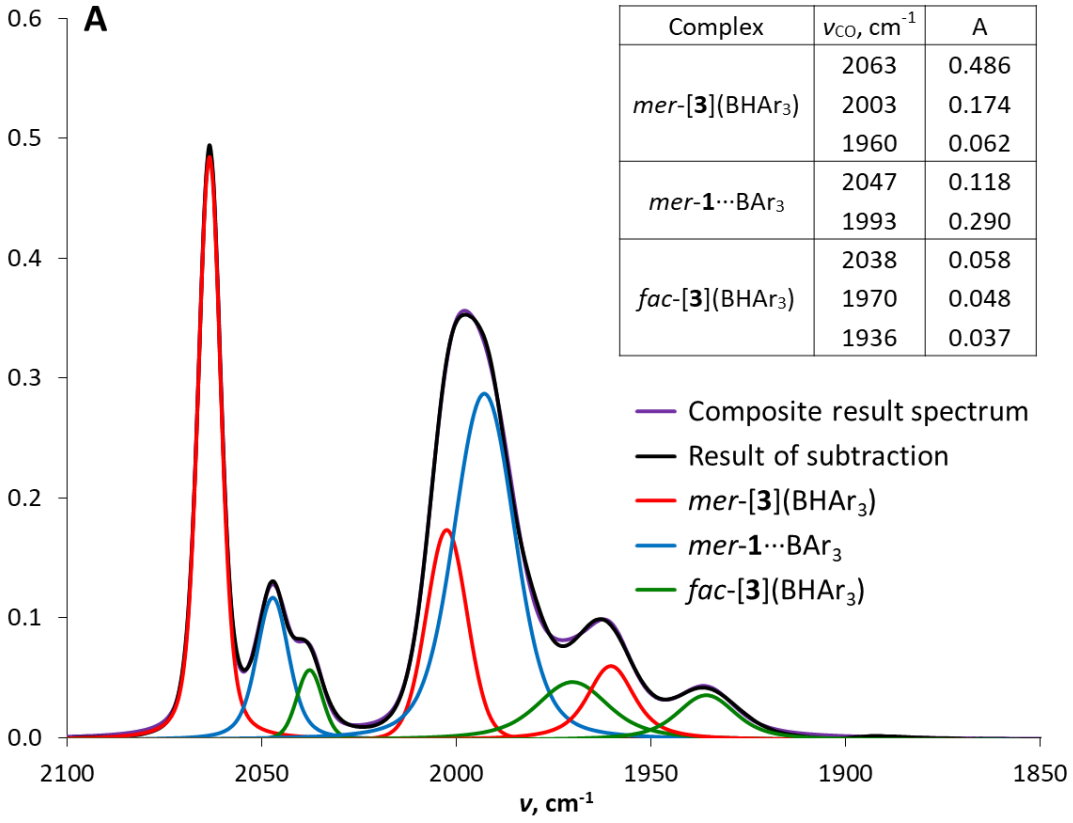

Complex	ν_{CO}, cm^{-1}	A
mer-[**3**](BHAr$_3$)	2063	0.486
	2003	0.174
	1960	0.062
mer-**1**···BAr$_3$	2047	0.118
	1993	0.290
fac-[**3**](BHAr$_3$)	2038	0.058
	1970	0.048
	1936	0.037

Figure S3. IR spectrum of the mixture *of fac*-**1** with 1.5 equiv. of BAr_3 (Ar = C_6F_5) in CH_2Cl_2 at 180 K with the mathematical subtraction of the initial hydride spectrum and its peak deconvolution.

Determination of thermodynamic characteristics of hydride transfer from *fac*-1 to $B(C_6F_5)_3$ using low temperature IR studies.

For the reaction of *fac*-**1** with 1.3 equiv. of $B(C_6F_5)_3$ in toluene experimental equilibrium constants were obtained by IR spectroscopy at 210-240 K range (Figure S4, Table S1). Every temperature point was kept for 20 minutes. Thermodynamic parameters of hydride transfer ($\Delta H°$ = −3.3 kcal/mol, $\Delta S°$= 5.5 cal/(mol·K) were obtained by Van't-Hoff method from the $RlnK_p$ – 1/*T* dependency (Figure S5) according to the formula:

$$\Delta H/T - \Delta S = -R \cdot \ln K_p$$

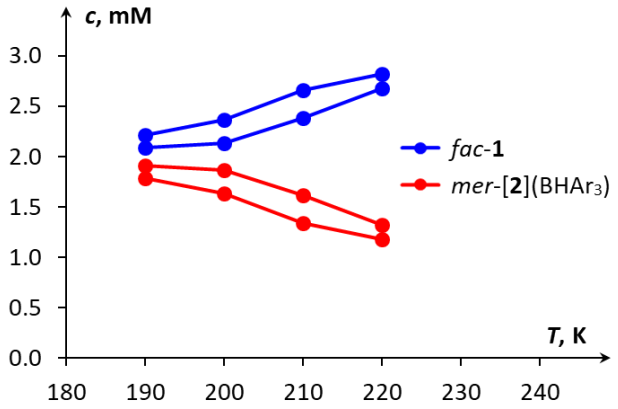

Figure S4. Temperature dependence of intensity of ν_{CO} bands of *fac*-**1** and *mer*-[**2**]($BHAr_3$) (Ar = C_6F_5). Experimental conditions: *fac*-**1** (*c* = 0.004 M), $B(C_6F_5)_3$ (*c* = 0.005 M), toluene, 190-220 K, *l* = 0.05 cm.

Table S1. Experimental equilibrium constants for *fac*-**1** + $B(C_6F_5)_3$ ↔ *mer*-[**2**]($BH(C_6F_5)_3$) process obtained from low temperature IR spectroscopy data.

T	1/*T*	*c*(*mer*-[**2**]$^+$)	*c*(*fac*-**1**)	*c*($B(C_6F_5)_3$)	*K*	*RlnK*
190	0.0053	0.0023	0.0017	0.0033	388	11.8
200	0.0050	0.0019	0.0021	0.0037	233	10.8
210	0.0048	0.0016	0.0024	0.0040	170	10.2
220	0.0045	0.0013	0.0027	0.0043	116	9.4

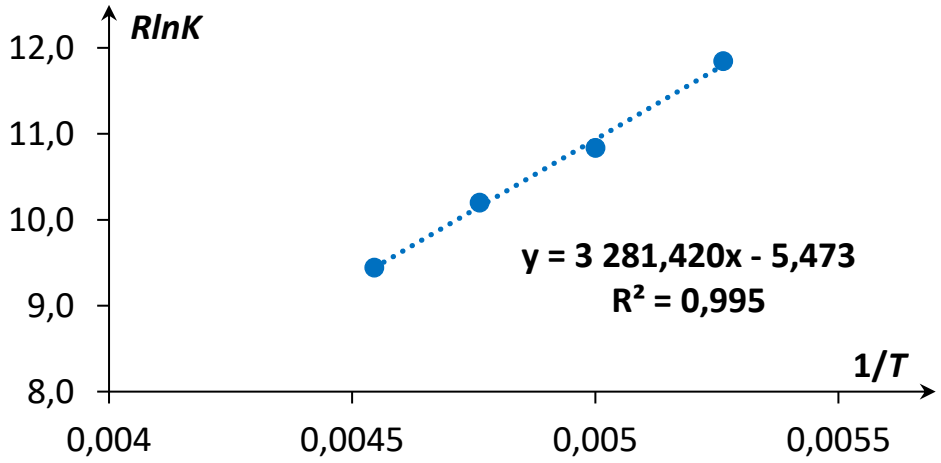

Figure S5. RlnK *vs.* 1/T plot for determination of thermodynamic parameters for hydride transfer.

Determination of kinetic parameters of hydride transfer from *fac*-1 and *fac*-1-d_3 to $B(C_6F_5)_3$ using low temperature IR studies

The interaction between *fac*-[(dppm)Mn(CO)$_3$H] (*fac*-**1**) and BAr_3 (Ar = C_6F_5) as a Lewis acid could be described as the second order reaction with two pre-equilibria (K_1 and K_2, see below), since the formation of *mer*-[(dppm)Mn(CO)$_3$(κ^1(Cl)-*n*BuCl)](BAr_4) (*mer*-[**3'**]$^+$) is reversible at low temperatures, and warming from 160 K to 190 K shifts this equilibrium to the formation of initial manganese hydride *fac*-**1**. At the same time, the *mer*-to-*fac* isomerization of *mer*-[**3'**]$^+$ is almost irreversible due to much higher stability of *fac*-[(dppm)Mn(CO)$_3$(κ^1(Cl)-*n*BuCl)](BAr_4) (*fac*-[**3'**]$^+$). Excluding the process of *fac*-to-*mer* isomerization for starting hydrides **1** and hydrogen bonded adducts **1**···BAr_3, the mechanism could be simplified to following scheme with appropriate kinetic equations. Taking into account that the rate-determining step is *mer*-[**3'**]$^+$ → *fac*-[**3'**]$^+$ isomerization, the overall process rate will be $r = k$[*mer*-[**3'**]$^+$], where concentration of *mer*-[**3'**]$^+$ could be expressed like *mer*-[**3'**]$^+$ = K_1K_2[**1**][BAr_3]. The reaction rate in this case will be $r = k_{eff}$[$\mathbf{1}^H$][BAr_3], in which $k_{eff} = K_1K_2k$.

$$\mathbf{1} + BAr_3 \overset{K_1}{\rightleftharpoons} \mathbf{1}\cdots BAr_3 \qquad K_1 = \frac{[\mathbf{1}\cdots BAr_3]}{[\mathbf{1}]\,[BAr_3]} \qquad K_2 = \frac{[mer\text{-}[\mathbf{3'}]^+]}{[\mathbf{1}\cdots BAr_3]} \qquad r = k[mer\text{-}[\mathbf{3'}]^+]$$

$$\mathbf{1}\cdots BAr_3 \overset{K_2}{\rightleftharpoons} mer\text{-}[\mathbf{3}]^+$$

$$mer\text{-}[\mathbf{3}]^+ \xrightarrow{k} fac\text{-}[\mathbf{3}]^+$$

$$r = k\,K_1\,K_2\,[\mathbf{1}]\,[BAr_3] = k_{eff}\,[\mathbf{1}]\,[BAr_3]$$

Experimental effective rate constants for the reaction of *fac*-**1** with 1.2 equiv. of BAr_3 (Table S2) were obtained in *n*BuCl at 220-250 K temperature range with integrated rate equation for second order reaction when initial reagents concentrations are not equal:

$$kt = \frac{\mathbf{1}}{[\mathbf{1}]_0[BAr_3]_0} \ln \frac{[BAr_3]_0[\mathbf{1}]}{[\mathbf{1}]_0[BAr_3]}$$

Then the corresponding activation parameters (Figure S6) were calculated with Eyring's equation for bimolecular reaction in solution (see below). Analysis of the experimental data for *fac*-**1** and *fac*-**1**-d_3 under the same conditions at 230 K (Figure S7) revealed the negligible kinetic isotopic effect (k_H/k_D = 0.9 ± 0.1).

$$k_{eff} = \frac{k_B T}{\hbar} e^{-\frac{\Delta H}{RT} + \frac{\Delta S}{T}}$$

Table S2. Experimentally determined effective rate constants for the interaction between *fac*-**1** and 1.2 equiv. of BAr_3 in *n*BuCl at 220-250 K range.

	$k_{eff} = K_1K_2k$, s·M^{-1}
T, K	*fac*-**1**/$B(C_6F_5)_3$
220	$2.4 \cdot 10^{-3}$
230	$6.9 \cdot 10^{-3}$
240	$1.9 \cdot 10^{-2}$
250	$4.4 \cdot 10^{-2}$

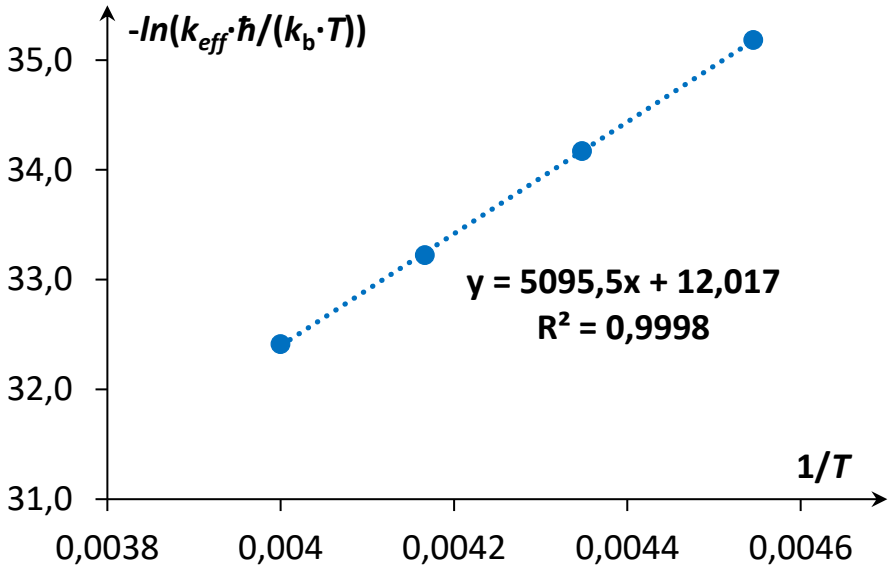

Figure S6. $-\ln(k_{eff}\cdot\hbar/(T\cdot k_B))$ *vs* $1/T$ plot used for the determination of activation parameters for hydride transfer.

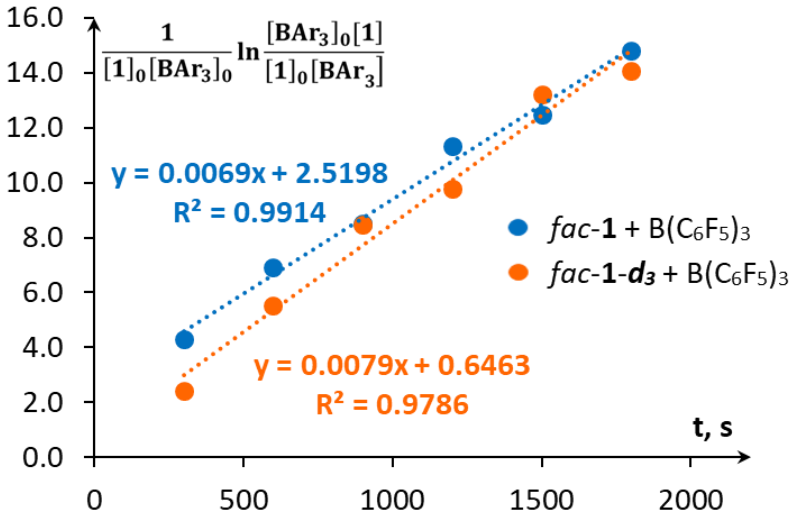

$\Delta H^{\neq}$, kcal/mol	10.1 ± 0.5
$\Delta S^{\neq}$, cal/(mol·K)	−24 ± 2
$\Delta G_{230}^{\neq}$, kcal/mol	15.6

Figure S7. $-\ln(k_{eff}\cdot\hbar/(T\cdot k_B))$ *vs t* plots for the determination of effective rate constants of for hydride (*fac*-**1** + $B(C_6F_5)_3$, blue) and deuteride (*fac*-**1**-d_3 + $B(C_6F_5)_3$, orange) transfer processes at 230K.

General procedure for variable temperature NMR experiments

A solution of *fac*-[(dppm)Mn(CO)$_3$H] (*fac*-**1**) (20 mg, 0.04 mmol) in CD_2Cl_2 (0.2 mL) was filtered through Celite directly into the NMR tube and the filter pad was washed with additional amount of solvent (0.1 mL). The resulting solution was frozen in a liquid nitrogen and the solution of corresponding Lewis acid ([Ph_3C][$B(C_6F_5)_4$]: 36.9 mg, 1 equiv.; $B(C_6F_5)_3$: 20 mg, 1 equiv.) in CD_2Cl_2 (0.2 mL) was carefully added on the wall of frozen NMR tube. Two frozen solutions were simultaneously melted and mixed in slush liquid nitrogen/EtOH bath at *ca.* 180 K and the resulting NMR sample was inserted into pre-cooled NMR probe at 183 K and then monitored with multi-nuclear NMR spectroscopy in 183-273 K temperature range.

NMR spectroscopy characterization of Mn(I) cationic complexes *fac*-[3](BAr$_4$), *mer*-[4](BAr$_4$), *fac*-[5](BAr$_4$) and *fac*-[2](HBAr$_3$).

Spectroscopic characterization of complex *fac*-[3](B(C$_6$F$_5$)$_4$).

The most pertinent NMR spectra for this compound are shown in Figures S13-S15. Based on ^{1}H and ^{31}P NMR data complex *fac*-[**3**](B(C$_6$F$_5$)$_4$) exists in solution as a mixture of two isomers in *ca.* 4:1 ratio at room temperature attributed to *fac,anti*- (**A**, major) and *fac,syn*- (**B**, minor) forms according to the results of DFT calculations (see page S41). The equivalent amount of Ph$_3$CH was also observed in ^{1}H and ^{13}C spectra, but their signals in ^{1}H and ^{13}C spectra are not listed.

***fac*-[3](B(C$_6$F$_5$)$_4$):**

^{1}H NMR (600.1 MHz, CD_2Cl_2, 298 K) δ 7.47-7.08 (m, 20H, C*H*$_{Ar}$, **A**+**B**), 5.05 (dt overlapped with another dt, $^2J_{HH}$ = 16.3 Hz, $^2J_{PH}$ = 11.7 Hz, 0.2H, PC*H*$_2$P, **B**), 5.03 (dt overlapped with another dt, $^2J_{HH}$ = 16.4 Hz, $^2J_{PH}$ = 11.5 Hz, 0.8H, PC*H*$_2$P, **A**), 4.78 (dt, $^2J_{HH}$ = 16.4 Hz, $^2J_{PH}$ = 11.5 Hz, 0.8H, PC*H*$_2$P, **A**), 4.66 (dt, $^2J_{HH}$ = 16.3 Hz, $^2J_{PH}$ = 11.7 Hz, 0.2H, PC*H*$_2$P, **B**).

^{1}H{^{31}P} NMR (600.1 MHz, CD_2Cl_2, 298 K) δ 7.08-7.47 (m, C*H*$_{Ar}$, **A**+**B**), 5.05 (d overlapped with another d, $^2J_{HH}$ = 16.2 Hz, PC*H*$_2$P, **B**), 5.03 (d overlapped with another d, $^2J_{HH}$ = 16.3 Hz PC*H*$_2$P, **A**), 4.78 (d, $^2J_{HH}$ = 16.3 Hz, PC*H*$_2$P, **A**), 4.66 (d, $^2J_{HH}$ = 16.2 Hz, PC*H*$_2$P, **B**).

^{31}P{^{1}H} NMR (243.0 MHz, CD_2Cl_2, 298 K): δ 13.8 (s, **B**), 10.0 (s, **A**).

^{13}C{^{1}H} NMR (150.9 MHz, 243 K, CD_2Cl_2): 219.7 (t, $^2J_{PC}$ = 18.8 Hz, Mn–*C*O, **A**), 215.2 (br s, Mn–*C*O, **B**), 214.8 (br s, Mn–*C*O, **A**), 147.9 (br d, $^1J_{BF}$ = 239.5 Hz, *C*$_{ortho}$ B(C$_6$F$_5$)$_4$), 138.1 (br dt, $^1J_{BF}$ = 239.5 Hz, $^2J_{BF}$ = 11.5 Hz, *C*$_{para}$ B(C$_6$F$_5$)$_4$), 136.2 (br d, $^1J_{BF}$ = 245.7 Hz, *C*$_{meta}$ B(C$_6$F$_5$)$_4$), 133.0, 132.9 (s, *C*H$_{PPh_2}$, **B**), 132.7, 132.5 (s, *C*H$_{PPh_2}$, **A**), 131.5 (vt, J_{PC} = 5.9 Hz, *C*H$_{PPh_2}$, **B**), 131.3 (vt, J_{PC} = 5.6 Hz, *C*H$_{PPh_2}$, **A**), 131.0 (vt, J_{PC} = 5.3 Hz, *C*H$_{PPh_2}$, **A**), 130.9 (vt, J_{PC} = 5.8 Hz, *C*H$_{PPh_2}$, **B**), 130.6 (vt, J_{PC} = 4.9 Hz, *C*H$_{PPh_2}$, **B**), 130.4 (vt, J_{PC} = 5.7 Hz, *C*H$_{PPh_2}$, **B**), 130.3 (vt, J_{PC} = 5.2 Hz, *C*H$_{PPh_2}$, **A**), 130.1 (vt, J_{PC} = 5.3 Hz, *C*H$_{PPh_2}$, **A**), 129.6 (vt, J_{PC} = 25.2 Hz, C$_{ipso\text{-}PPh_2}$, **A**), 127.2 (vt, J_{PC} = 19.4 Hz, C$_{ipso\text{-}PPh_2}$, **A**), 123.6 (br m, C$_{ipso}$ B(C$_6$F$_5$)$_4$), 63.0 (br m, Mn−*C*D$_2$Cl$_2$, **A**+**B**), 39.7 (t, $^1J_{PC}$ = 24.3 Hz, P*C*H$_2$P, **A**+**B**).

IR (CH_2Cl_2, 290 K): ν_{CO} 2037, 1968, 1946 cm^{-1}; IR (*n*BuCl, 290 K): ν_{CO} 2040, 1970, 1943 cm^{-1}; IR (toluene, 290 K): ν_{CO} 2037, 1967, 1942 cm^{-1}.

Characterization of complex *mer*-[4](B(C$_6$F$_5$)$_4$) observed by low-temperature NMR monitoring of the reaction between *fac*-1 and [Ph$_3$C](B(C$_6$F$_5$)$_4$).

The approximate ratio between *mer*-[**4**](B(C$_6$F$_5$)$_4$), *fac,anti*-[**3**](B(C$_6$F$_5$)$_4$) and Ph$_3$CH in the reaction mixture at 183 K was determined by the integration for well-separated signals at δ_H 5.78, 4.74 and 5.58 ppm, respectively (Figure S18). A quantitative ^{1}H NMR yield of two latter products was observed at 223 K using the signal of residual solvent protons as an internal standard (Figure S18, inset). The existence of CH=CHCH$_2$CH=CH structural motif in the molecule of *mer*-[**4**](B(C$_6$F$_5$)$_4$) was unambiguously confirmed by ^{1}H TOCSY NMR spectrum (Figure S20) and their exact attribution was inferred using ^{1}H–^{1}H COSY (Figure S19) and ^{1}H–^{13}C HSQC (Figure S23) spectra. Based on the general trends known in the literature, it was proposed that more upfield CH resonances observed at δ_H/δ_c 5.78/107.4 and 4.41/88.5 ppm belong to the CH=CH moiety coordinated to the manganese atom (Figures S22-23), whereas non-coordinated CH=CH 1,4-cyclohexadiene fragment was attributed to the signals at δ_H/δ_c 6.44/126.5 and 5.51/127.7 ppm. Upon warming a fast transformation of *mer*-[**4**](B(C$_6$F$_5$)$_4$) into *fac*-[**3**](B(C$_6$F$_5$)$_4$) was observed by ^{1}H and ^{31}P NMR spectroscopy (Figure S24-S25) together with a detection of non-coordinated cyclic diene **5** isomerizing into triphenylmethane.

***mer*-[4](B(C$_6$F$_5$)$_4$):**

^{1}H NMR (600.1 MHz, CD_2Cl_2, 183 K): δ 7.72 (br dd, J_{PH} = 12.2, $^3J_{HH}$ = 7.3 Hz, 2H, C*H*$_{PPh_2}$), 7.67-7.28 (m, overlapped with signals of *fac*-[**3**](B(C$_6$F$_5$)$_4$), 24H, C*H*$_{PPh_2}$+C*H*$_{Ph}$), 6.98 (d, $^3J_{HH}$ = 7.3 Hz, 2H, C*H*$_{Ph}$), 6.87 (br dd, J_{PH} = 11.4, $^3J_{HH}$ = 7.5 Hz, 2H, C*H*$_{PPh_2}$), 6.44 (d, $^3J_{HH}$ = 10.5 Hz, 1H, CH$_2$CH=C*H*), 5.78 (br d, $^3J_{HH}$ = 8.5 Hz, 1H,

$CH_2CH=CH$...Mn), 5.51 (br d, $^3J_{HH}$ = 10.8 Hz, 1H, CH_2CH=CH), 5.05 (dt, $^2J_{HH}$ = 18.0 Hz, $^2J_{PH}$ = 9.3 Hz, 1H, PCH_2P), 4.53-4.40 (m overlapped with singlet, 2H, PCH_2P+CH_2CH=CH...Mn), 2.23 (d, $^2J_{HH}$ = 25.7 Hz, 1H, CH_2), 2.06 (d, $^3J_{HH}$ = 25.7 Hz, 1H, $CH_2(CH=CH)_2$).

$^{31}P\{^1H\}$ NMR (243.0 MHz, 183 K, CD_2Cl_2): δ 10.6 (d, $^2J_{PP}$ = 44.4 Hz), 7.10 (d, $^2J_{PP}$ = 44.3 Hz).

$^{13}C\{^1H\}$ NMR (150.9 MHz, CD_2Cl_2, 183 K): δ 218.9 (br s, Mn–CO), 218.1 (br s, Mn–CO), 213.6 (br s, Mn–CO), 147.9 (br d, $^1J_{BF}$ = 238.5 Hz, C_{ortho} $B(C_6F_5)_4$), 140.2, 139.3 (s, $C_{ipso\text{-}Ph_2C=C}$), 138.1 (br dt, $^1J_{BF}$ = 239.0 Hz, $^2J_{BF}$ = 11.5 Hz, C_{para} $B(C_6F_5)_4$), 136.2 (br d, $^1J_{BF}$ = 245.7 Hz, C_{meta} $B(C_6F_5)_4$), 132.5-129.0 (numerous CH_{Ph} signals overlapping with those of *fac*-[**3**]($B(C_6F_5)_4$), 127.7 (s, CH_2CH=CH), 126.5 (s, CH_2CH=CH), 126.3 (vt, J_{PC} = 19.0 Hz, $C_{ipso\text{-}PPh_2}$), 125.7, 124.4 (s, $C_{Ph_2C=C}$), 123.6 (br m, C_{ipso} $B(C_6F_5)_4$), 107.6 (br s, CH_2CH=CH...Mn), 88.5 (br s, CH_2CH=CH...Mn), 39.8 (br d, $^1J_{PC}$ = 20 Hz, PCH_2P), 27.5 (br s, $CH_2(CH=CH)_2$).

IR (CH_2Cl_2, 180 K): ν_{CO} 2063 cm^{-1}; IR (*n*BuCl, 160 K): ν_{CO} 2064 cm^{-1}.

Compound 5: ^1H NMR (600.1 MHz, CD_2Cl_2, 213 K): δ 7.66-7.45 (m overlapped with signals of *fac*-[**3**]($B(C_6F_5)_4$), 20H, CH_{Ar}), 6.46 (d, $^3J_{HH}$ = 10.2 Hz, 2H, $CH_2(CH=CH)_2$), 5.88 (br dt, $^3J_{HH}$ = 9.2 Hz, 1H, $^3J_{HH}$ = 4.2 Hz, 2H, $CH_2(CH=CH)_2$), 3.07 (s, 2H, $CH_2(CH=CH)_2$).

Low temperature NMR monitoring of the reaction between complex *fac*-1 and $B(C_6F_5)_3$ and spectroscopic characterization of complexes *fac*-[3]($BH(C_6F_5)_3$) and *fac*-[2]($BH(C_6F_5)_3$).

The evidence of Lewis acid adducts formation by ^1H and ^{31}P NMR spectroscopy is illustrated in Figures S26 and S29, respectively. Several very broad signals presented in low-temperature ^1H NMR spectra in 5-to-3 ppm region (Figure 28) may be attributed to PCH_2P resonances of these adducts and/or cationic *mer*-[**3**]($BHAr_3$) intermediate involved into fluxional process. While two isomers of cationic *fac*-[**3**]($BHAr_3$) products (*ca.* 3:1 ratio at 183 K) attributed to *fac,anti-* (major, **A**) and *fac,syn-* (minor, **B**) forms according to the results of DFT calculations (see page S41) were observed in 183-233 K temperature range, these species at 243 K starts to transform into *fac*-[**2**]($BH(C_6F_5)_3$) being the principal component at 273 K. The spectroscopic characteristics of *fac*-[**3**](BAr_4) and *fac*-[**2**]($BH(C_6F_5)_3$) are quite similar and a sole notable difference between them deals with strong shielding of PCH_2P protons by 0.5-1.0 ppm in the latter (Figures S27-S28).

***fac*-[3]($BH(C_6F_5)_3$):**

^1H NMR (600.1 MHz, CD_2Cl_2, 183 K) δ 5.23 (dt, $^2J_{HH}$ = 16.7 Hz, $^2J_{PH}$ = 10.2 Hz, 0.7H, PCH_2P, **A**), 4.93-4.80 (m, 0.6H, PCH_2P, **B**), 4.76 (dt, $^2J_{HH}$ = 16.7 Hz, $^2J_{PH}$ = 11.9 Hz, 0.7H, PCH_2P, **A**).

$^1H\{^{31}P\}$ NMR (600.1 MHz, CD_2Cl_2, 183 K) δ 5.26 (d, $^2J_{HH}$ = 16.7 Hz, PCH_2P, **A**), 4.89 (d, $^2J_{HH}$ = 16.6 Hz, PCH_2P, **B**), 4.81 (d, $^2J_{HH}$ = 16.6 Hz, PCH_2P, **B**), 4.76 (d, $^2J_{HH}$ = 16.7 Hz, PCH_2P, **A**).

$^{31}P\{^1H\}$ NMR (243.0 MHz, CD_2Cl_2, 183 K): δ 11.1 (s, **B**), 10.1 (s, **A**).

***fac*-[2]($BH(C_6F_5)_3$):**

^1H NMR (600.1 MHz, CD_2Cl_2, 273 K) δ 7.46-7.36 (m, 12H, CH_{Ph}), 7.21-7.14 (m, 4H, CH_{Ph}), 7.12-7.06 (m, 4H, CH_{Ph}), 4.58 (dt, $^2J_{HH}$ = 15.6 Hz, $^2J_{PH}$ = 10.6 Hz, 1H, PCH_2P), 3.85 (dt, $^2J_{HH}$ = 15.6 Hz, $^2J_{PH}$ = 10.9 Hz, 1H, PCH_2P), 3.68 (very br, 1H, $BH(C_6F_5)_3$).

$^{31}P\{^1H\}$ NMR (243.0 MHz, CD_2Cl_2, 273 K): δ 10.1 (s).

^{11}B NMR (192.5 MHz, CD_2Cl_2, 273 K): δ 25.4 (br s).

$^{13}C\{^1H\}$ NMR (150.9 MHz, 253 K, CD_2Cl_2): 219.5 (t, $^2J_{PC}$ = 18.4 Hz, Mn–*C*O), 217.2 (br s, Mn–*C*O), 148.3 (br d, $^1J_{BF}$ = 243.6 Hz, C_{ortho} $BH(C_6F_5)_3$), 139.3 (br d, $^1J_{BF}$ = 248.0 Hz, C_{para} $BH(C_6F_5)_3$), 136.2 (br d, $^1J_{BF}$ = 245.7 Hz, C_{meta} $B(C_6F_5)_4$), 131.9 (vt, J_{PC} = 5.2 Hz, CH_{PPh_2}), 131.7, 131.5 (s, CH_{PPh_2}), 131.4 (vt, J_{PC} = 5.4 Hz, CH_{PPh_2}), 130.7 (vt, J_{PC} = 21.8 Hz, $C_{ipso\text{-}PPh_2}$), 130.4 (vt, J_{PC} = 20.0 Hz, $C_{ipso\text{-}PPh_2}$), 129.4 (vt overlapped with another vt, J_{PC} = 4.9 Hz, CH_{PPh_2}), 129.3 (vt overlapped with another vt, J_{PC} = 5.1 Hz, CH_{PPh_2}), 119.0 (br m, C_{ipso} $BH(C_6F_5)_3$), 38.4 (t, $^1J_{PC}$ = 20.6 Hz, PCH_2P).

IR (CH_2Cl_2, 290 K): ν_{CO} 2037, 1968, 1946 cm^{-1}; IR (*n*BuCl, 290 K): ν_{CO} 2040, 1970, 1943 cm^{-1}; IR (toluene, 290 K): ν_{CO} 2037, 1967, 1942 cm^{-1}.

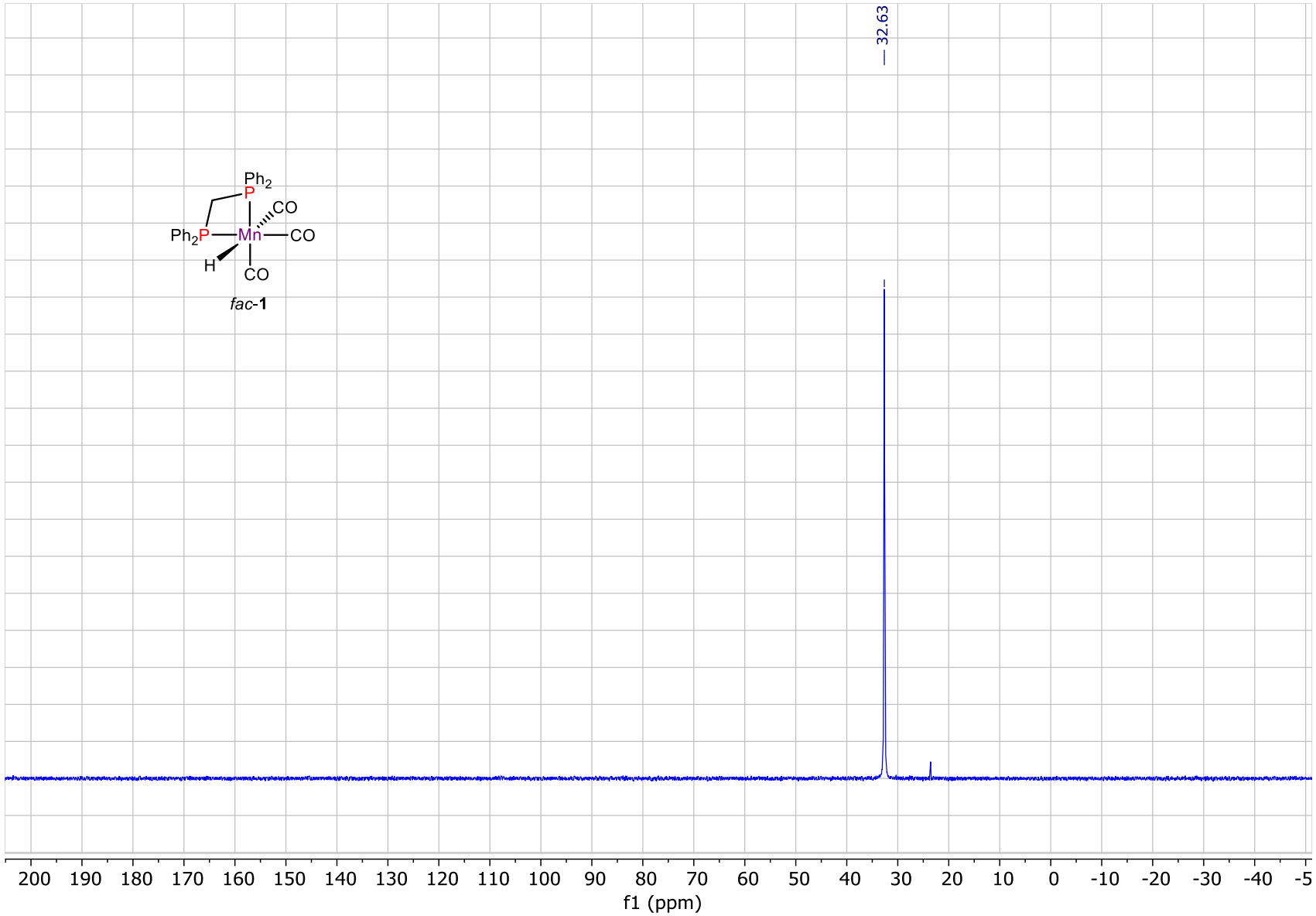

Figure S8. $^{31}P\{^{1}H\}$ NMR spectrum of complex *fac*-**1** (162.0 MHz, CD_2Cl_2, 298 K).

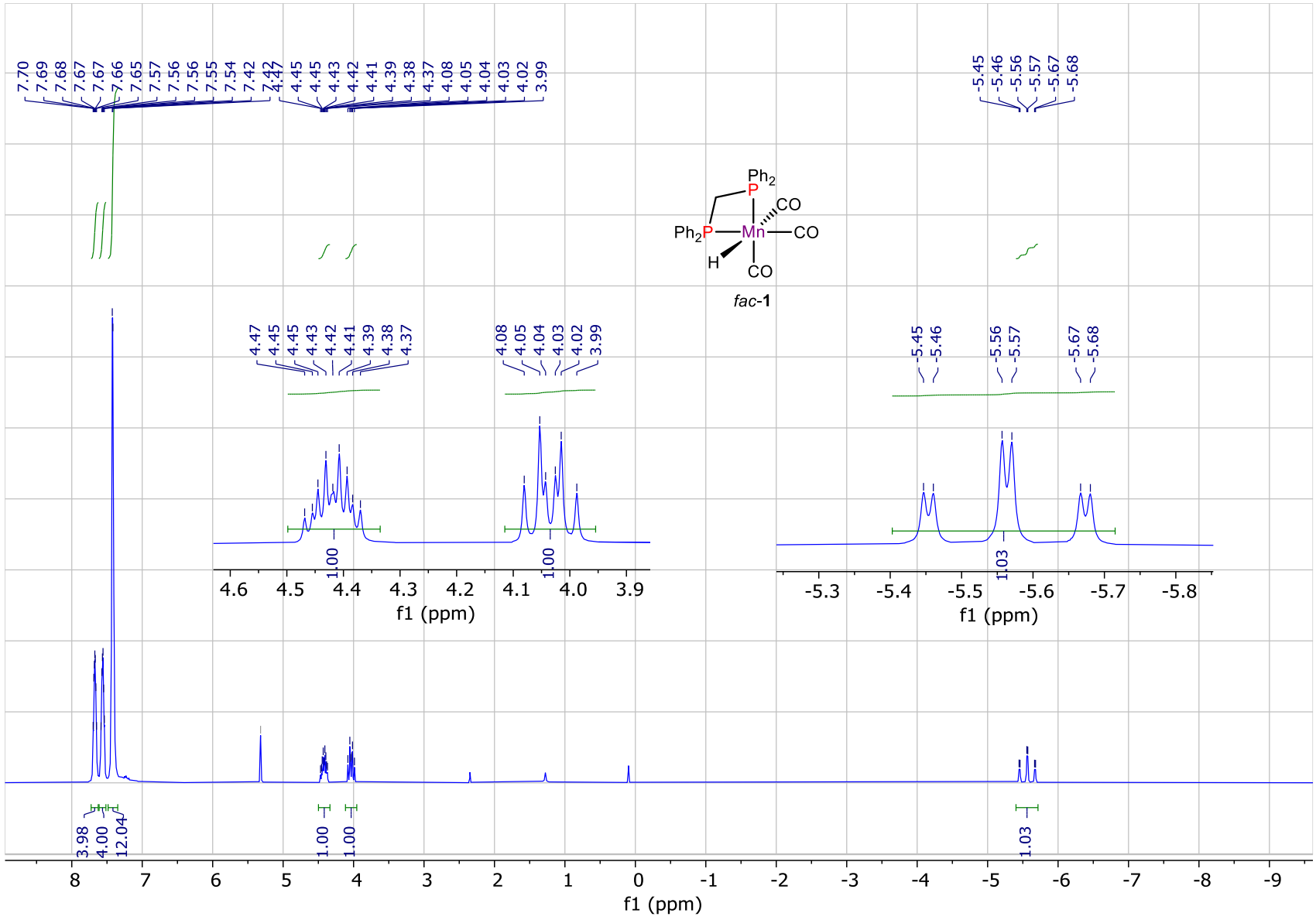

Figure S9. ^{1}H NMR spectrum of complex *fac*-**1** (400.1 MHz, CD_2Cl_2, 298 K).

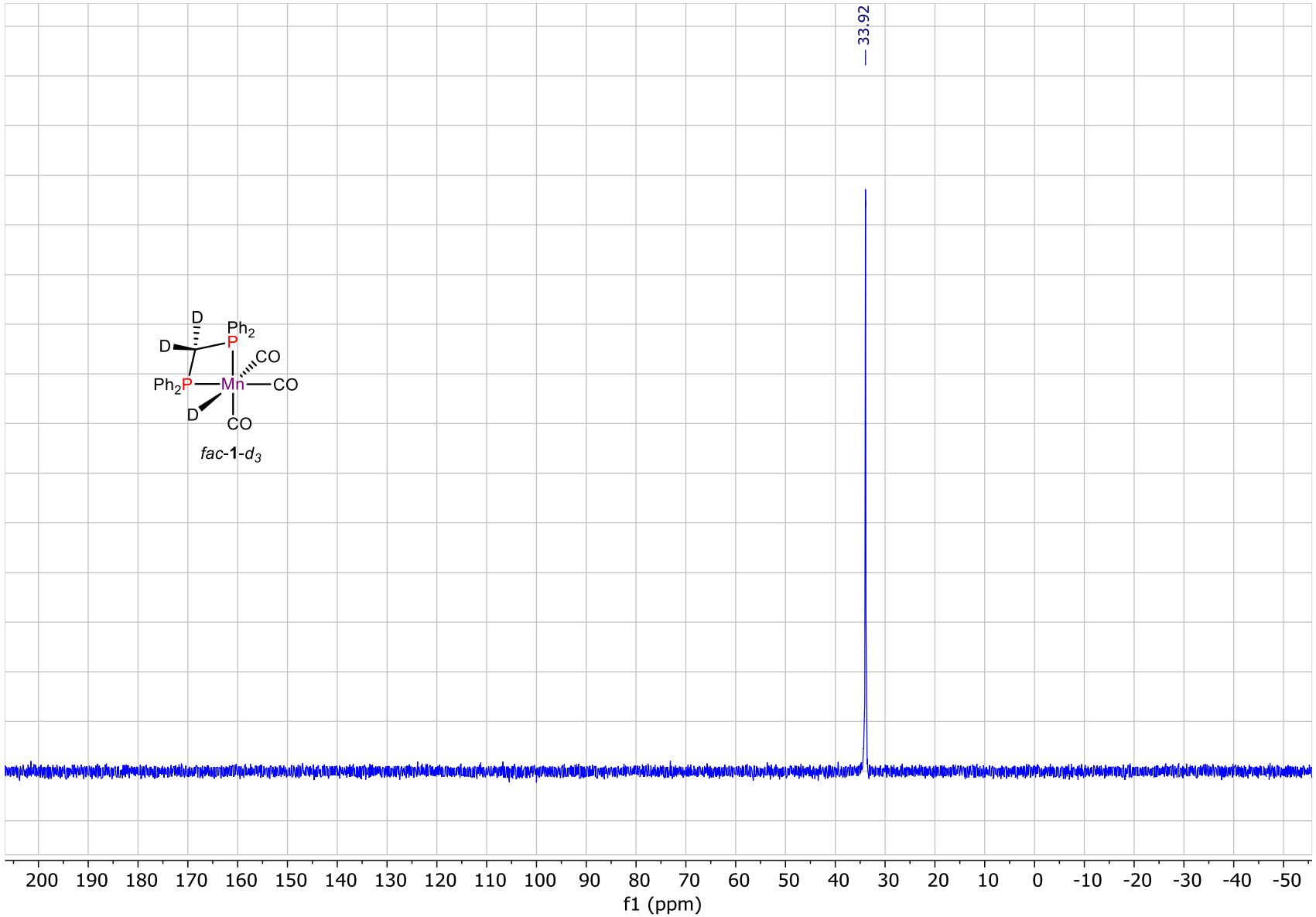

Figure S10. $^{31}P\{^{1}H\}$ NMR spectrum of complex *fac*-**1** (162.0 MHz, C_6D_6, 298 K).

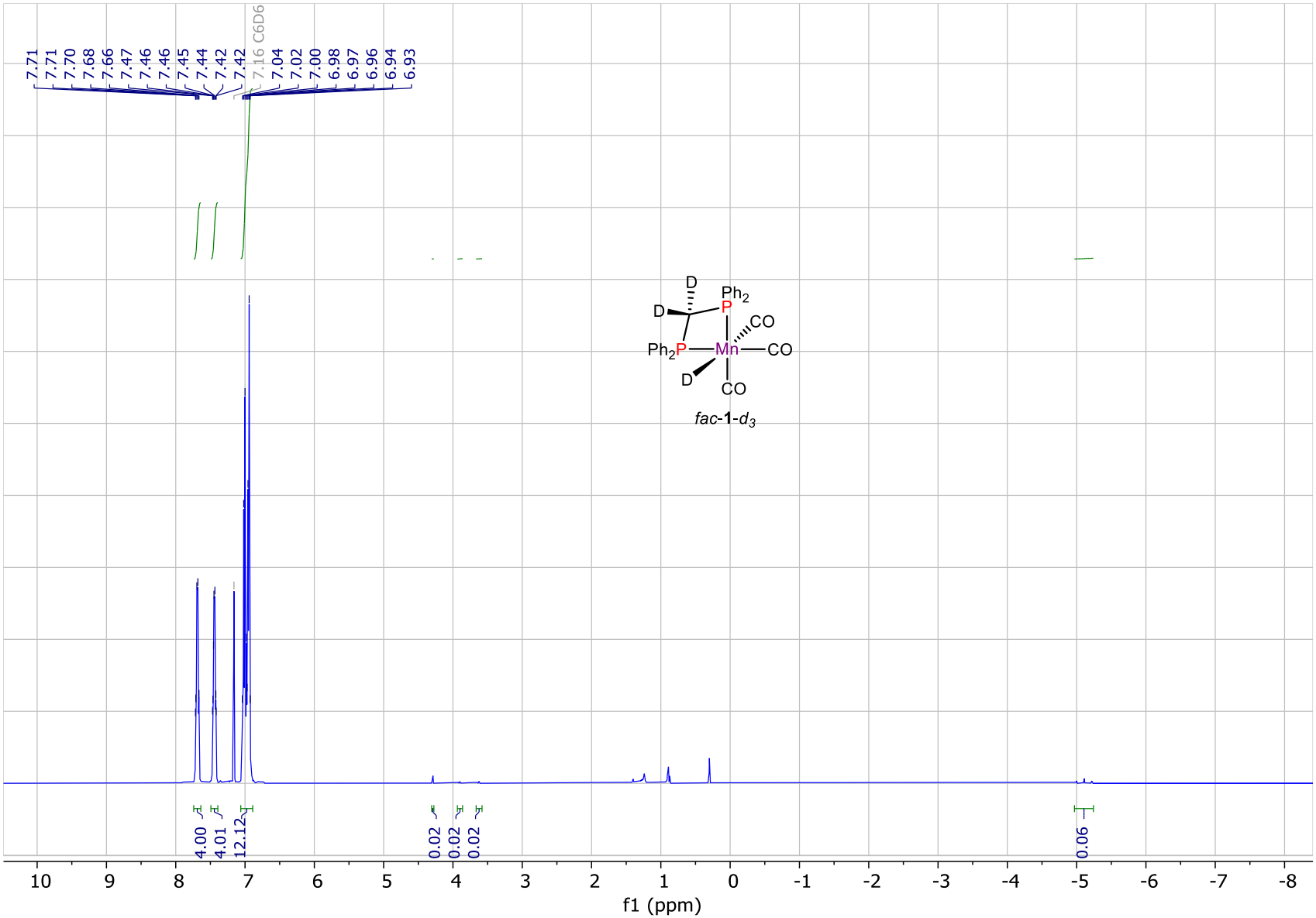

Figure S11. ^{1}H NMR spectrum of complex *fac*-**1**-d_3 (400.1 MHz, C_6D_6, 298 K).

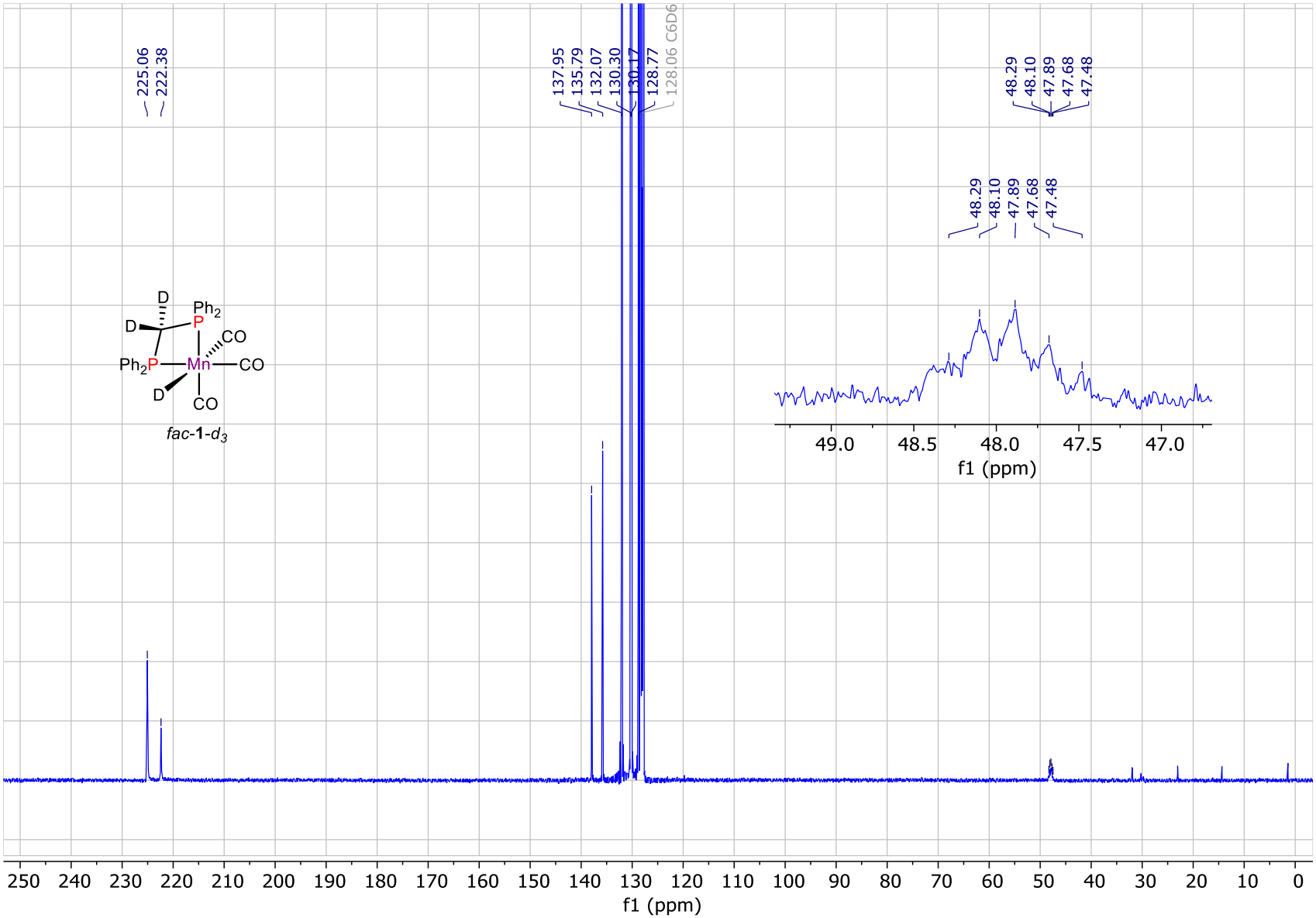

Figure S12. $^{13}C\{^{1}H,^{31}P\}$ NMR spectrum of complex *fac*-**1**-d_3 (100.6 MHz, C_6D_6, 298 K).

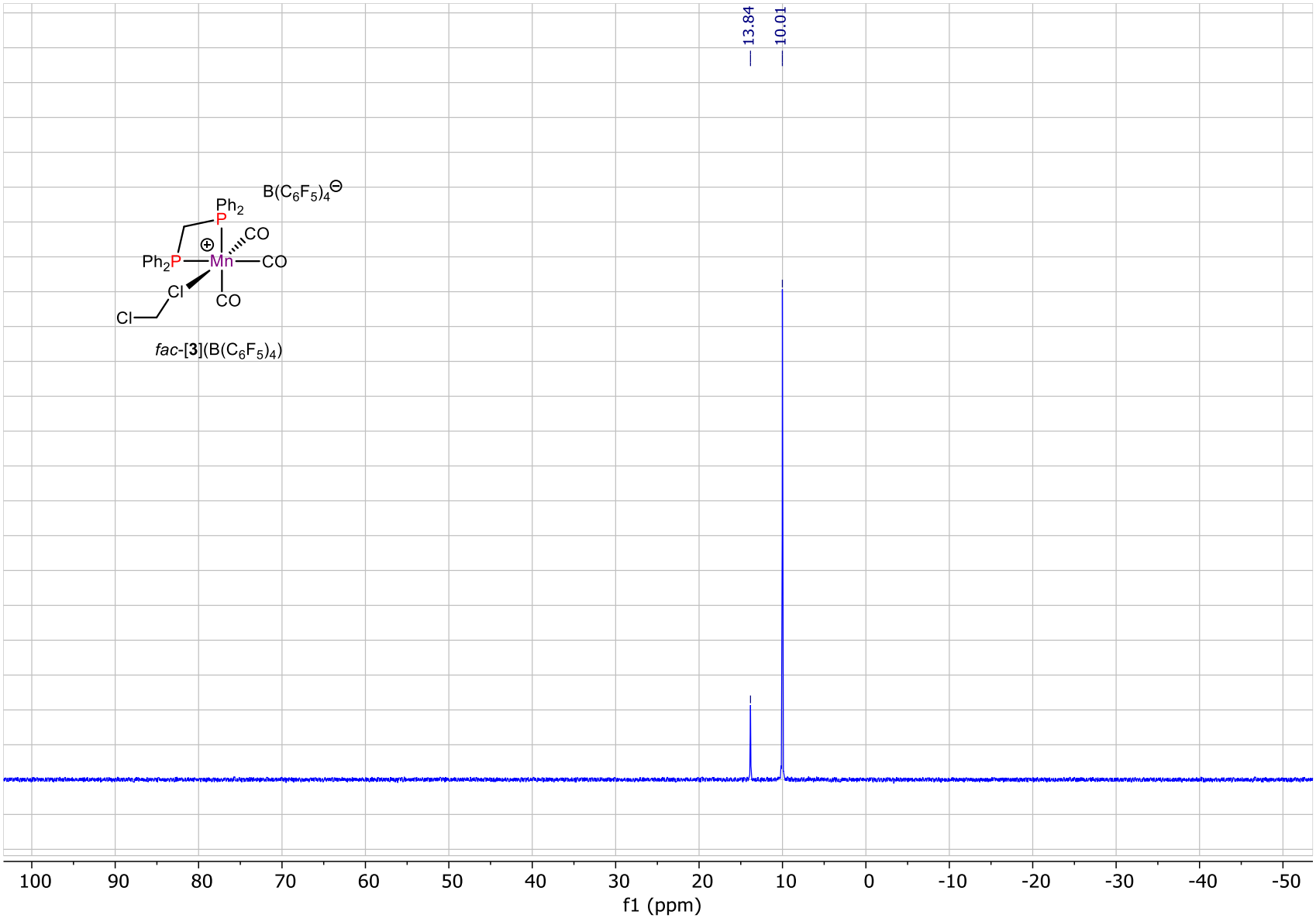

Figure S13. $^{31}P\{^{1}H\}$ NMR spectrum of complex *fac*-[**3**](B(C$_6$F$_5$)$_4$) (243.0 MHz, CD_2Cl_2, 298 K).

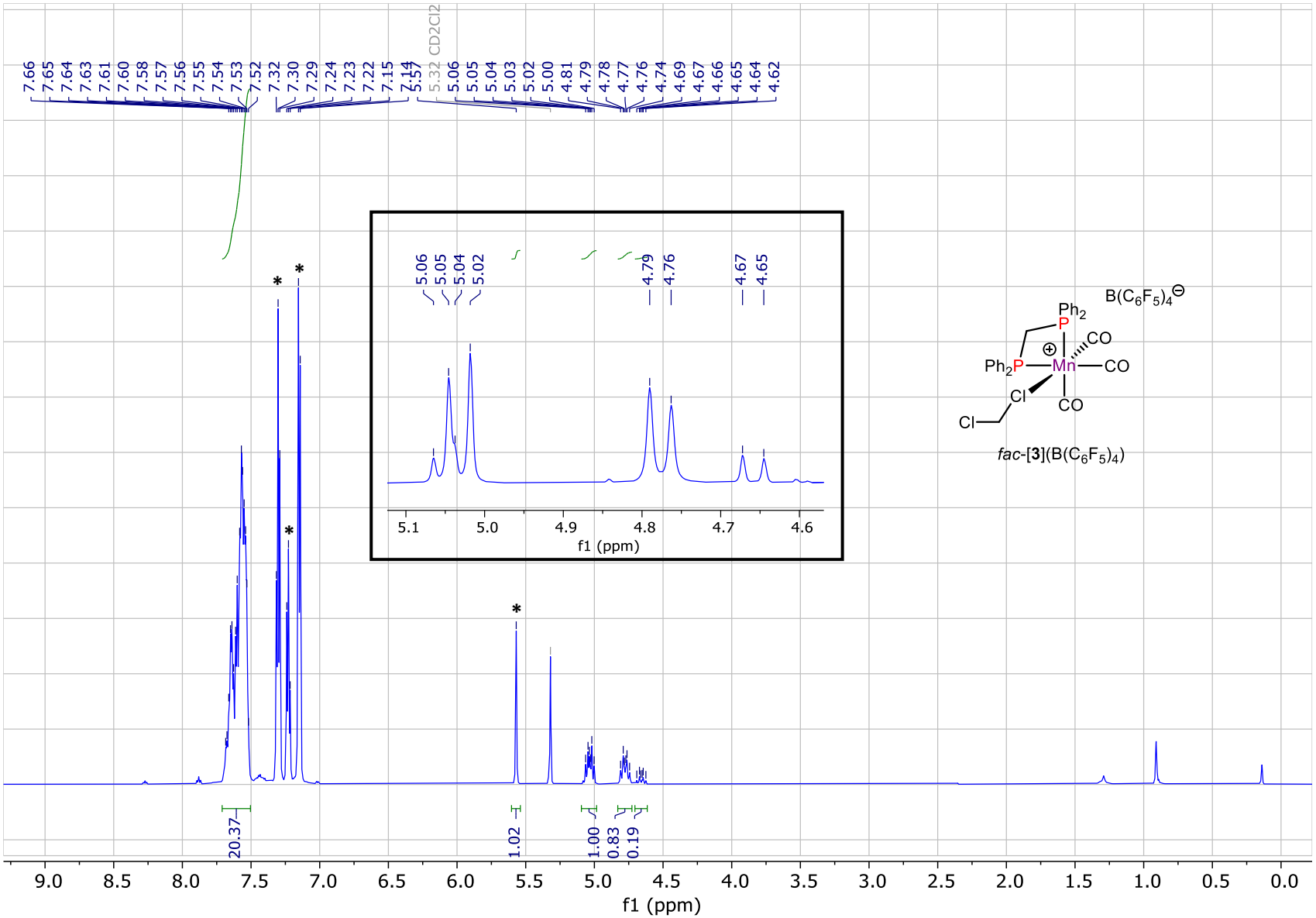

Figure S14. ^{1}H NMR spectrum of complex *fac*-[**3**](B(C$_6$F$_5$)$_4$) (600.1 MHz, CD_2Cl_2, 298 K), the signals of triphenylmethane are marked with asterisk. Inset spectrum corresponds to the section of PC*H*$_2$P protons in ^{1}H{^{31}P} decoupled experiment.

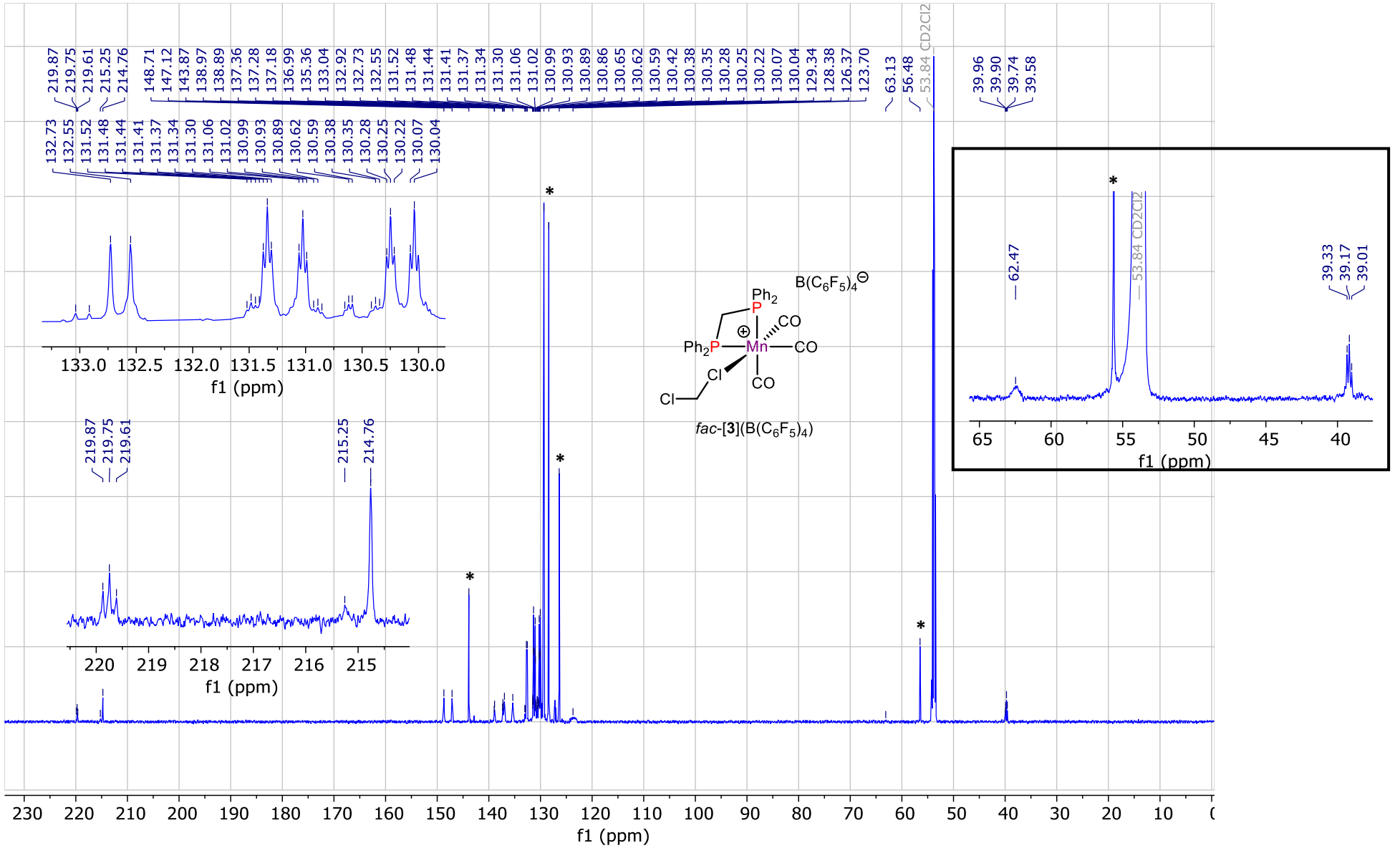

Figure S15. $^{13}C\{^{1}H\}$ NMR spectrum of complex *fac*-[**3**]$(B(C_6F_5)_4)$ (150.9 MHz, CD_2Cl_2, 243 K), the signals of triphenylmethane are marked with asterisk. Inset spectrum corresponds to the section of $^{13}C\{^{1}H\}$ NMR spectrum for the same compound at 183 K.

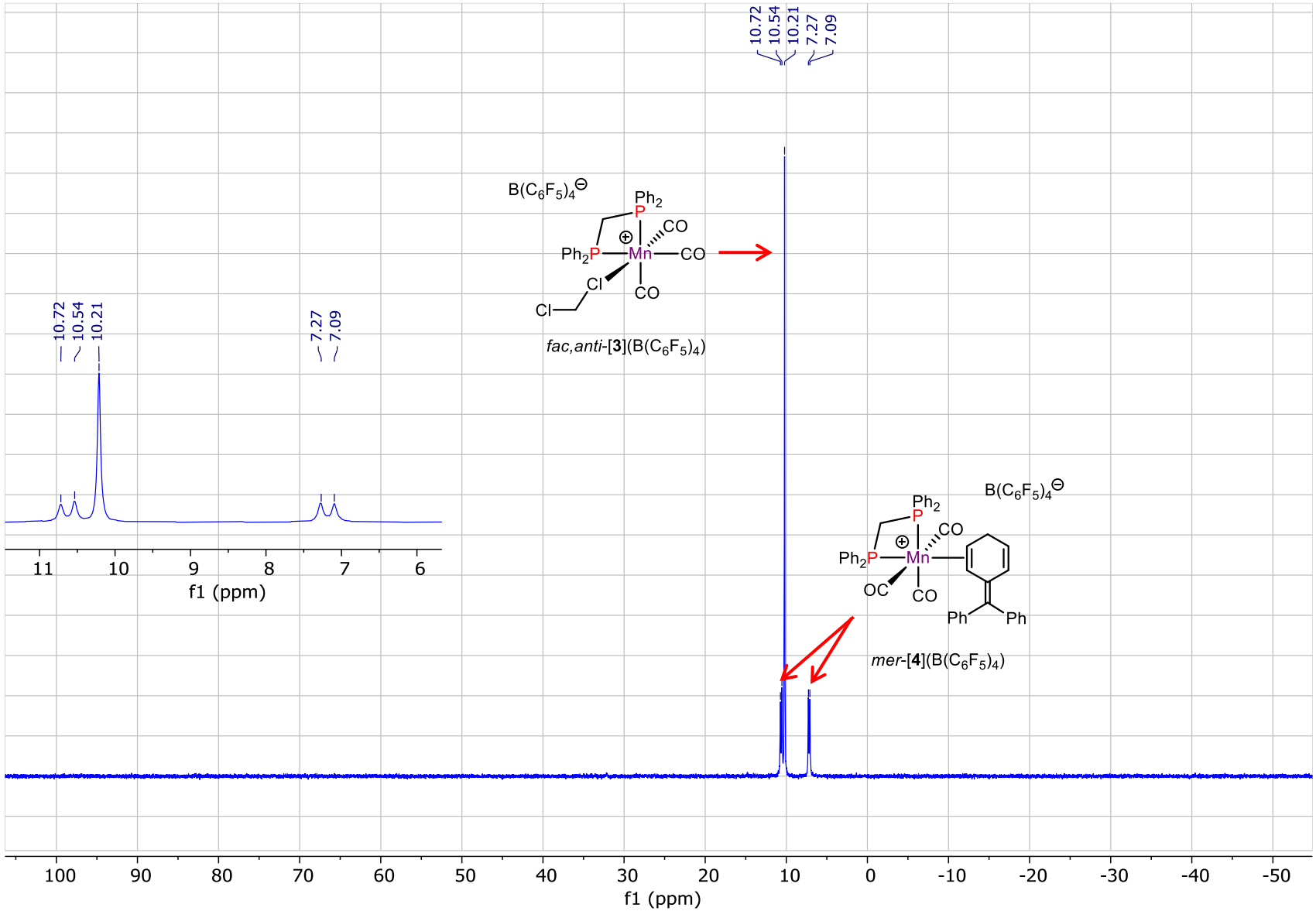

Figure S16. $^{31}P\{^{1}H\}$ NMR spectrum of the reaction between complex *fac*-**1** and $[Ph_3C](B(C_6F_5)_4)$ (243 MHz, CD_2Cl_2, 183 K).

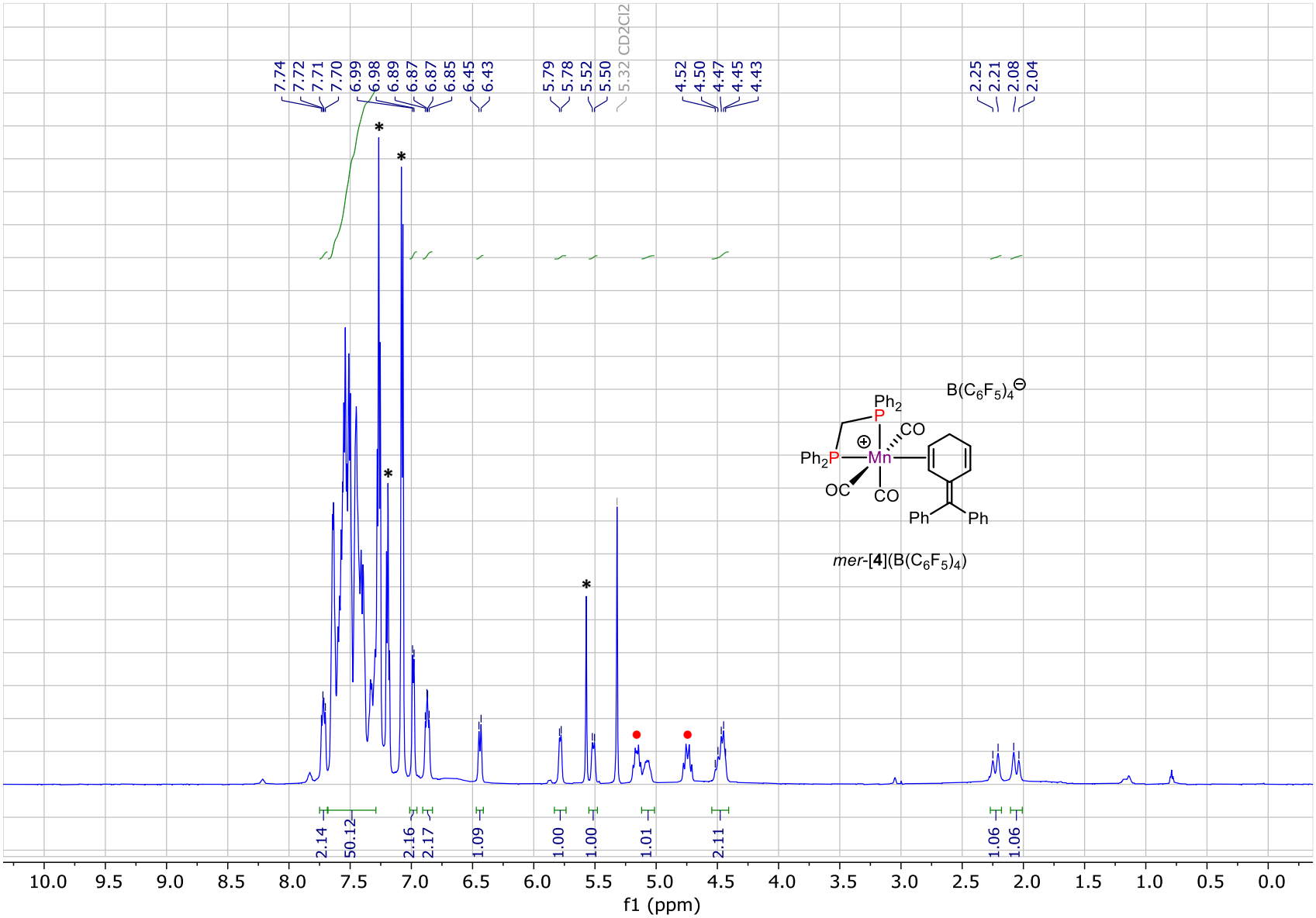

Figure S17. ^{1}H NMR spectrum of the reaction between complex *fac*-**1** and $[Ph_3C](B(C_6F_5)_4)$ (600.1 MHz, CD_2Cl_2, 183 K), only the signals of *mer*-[**4**]$(B(C_6F_5)_4)$ are identified and integrated. The signals of non-coordinated Ph_3CH are marked with asterisk, and those of *fac*-[**3**]$(B(C_6F_5)_4)$ with red dots.

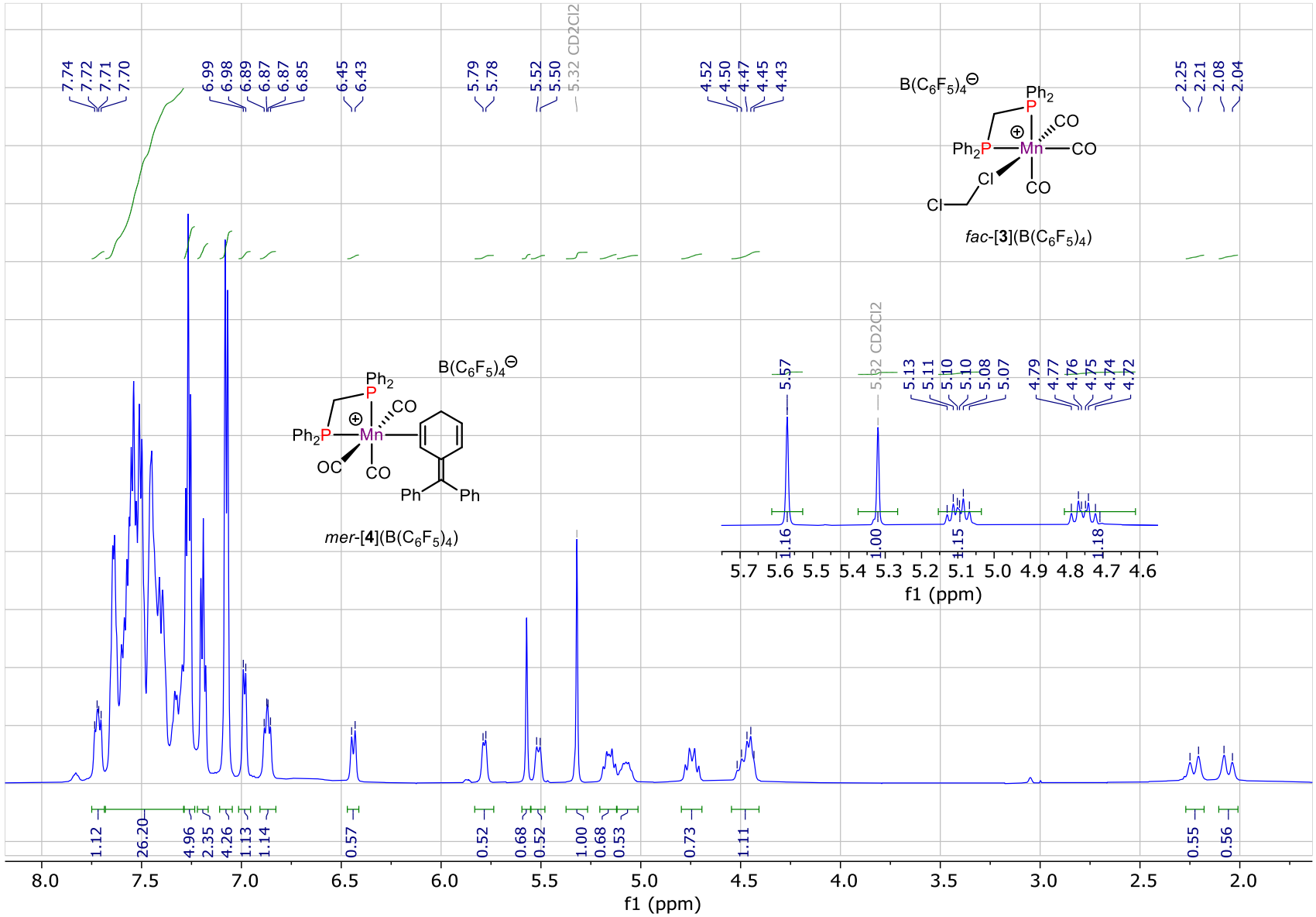

Figure S18. Section of ^{1}H NMR spectrum (600.1 MHz, CD_2Cl_2) of the mixture of *mer*-[**4**]($B(C_6F_5)_4$) and *fac*-[**3**]($B(C_6F_5)_4$) at 183 K indicating the amount of *fac*-[**2**]($B(C_6F_5)_4$) and free Ph_3CH (the signal of residual CD_2Cl_2 protons was used for internal standard). Inset corresponds to the sample after full conversion into *fac*-[**3**]($B(C_6F_5)_4$) at 223 K.

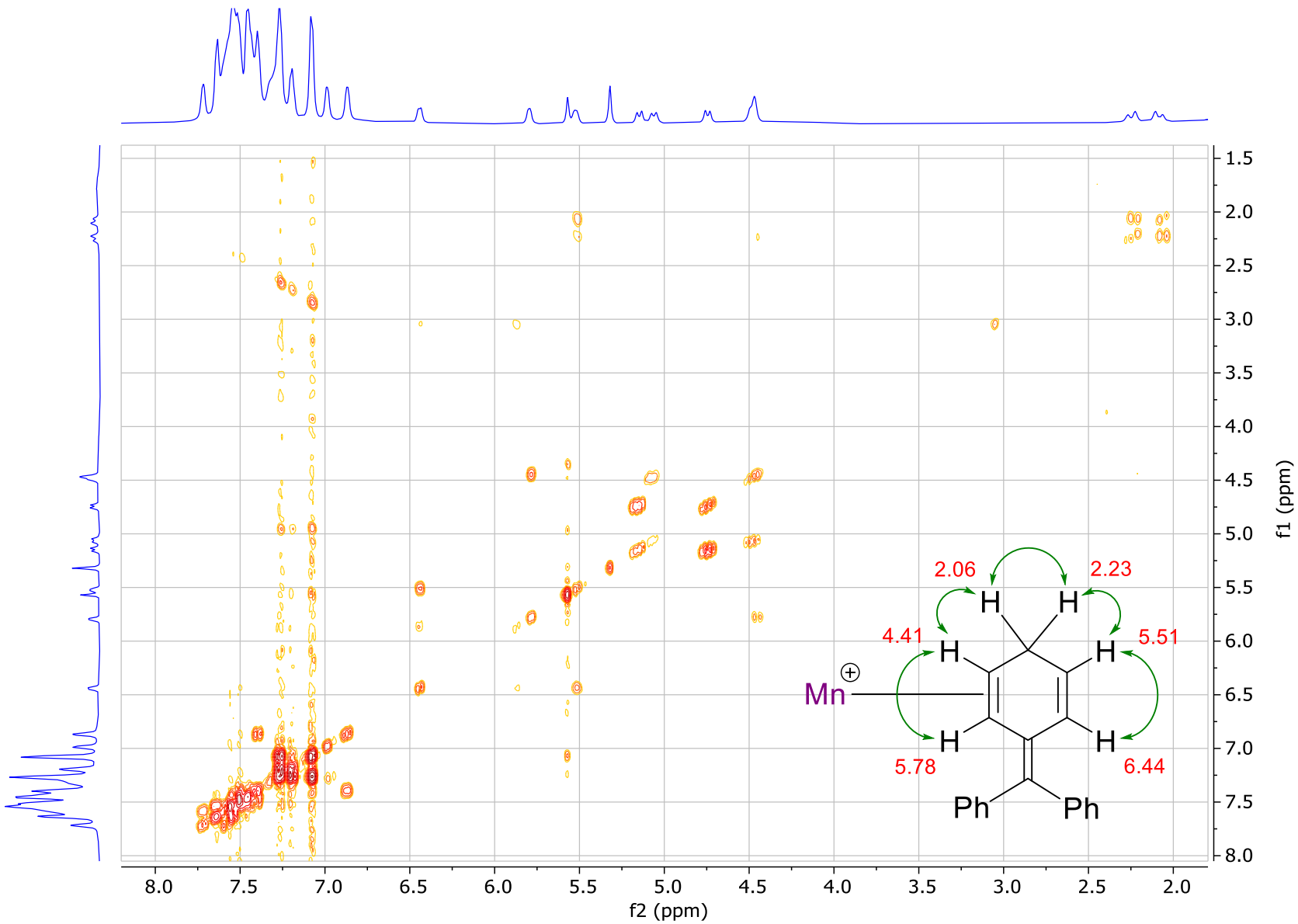

Figure S19. $^{1}H–^{1}H$ COSY NMR spectrum with ^{31}P decoupling of the reaction between complex *fac*-**1** and $[Ph_3C](B(C_6F_5)_4)$ (600.1 MHz, CD_2Cl_2, 183 K) and correlation scheme in 1,4-cyclohexadiene moiety (chemical shifts are shown in red and the observed correlation between the corresponding protons with green arrows).

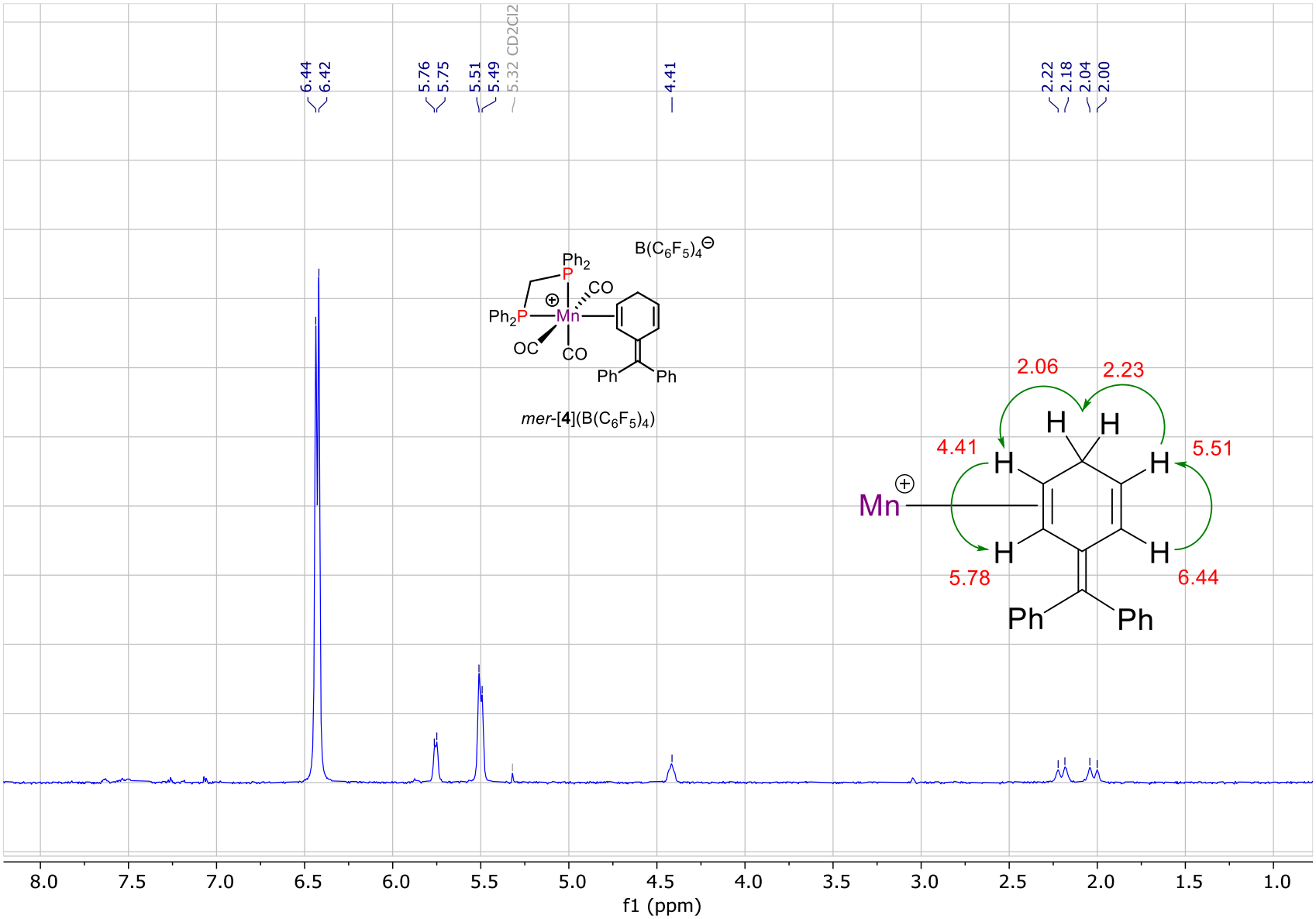

Figure S20. 1D ^{1}H TOCSY spectrum of *mer*-[**4**](B(C$_6$F$_5$)$_4$) (600.1 MHz, CD_2Cl_2, 183 K, irradiated at 6.44 ppm) and proposed scheme of spin transfer (green arrows)

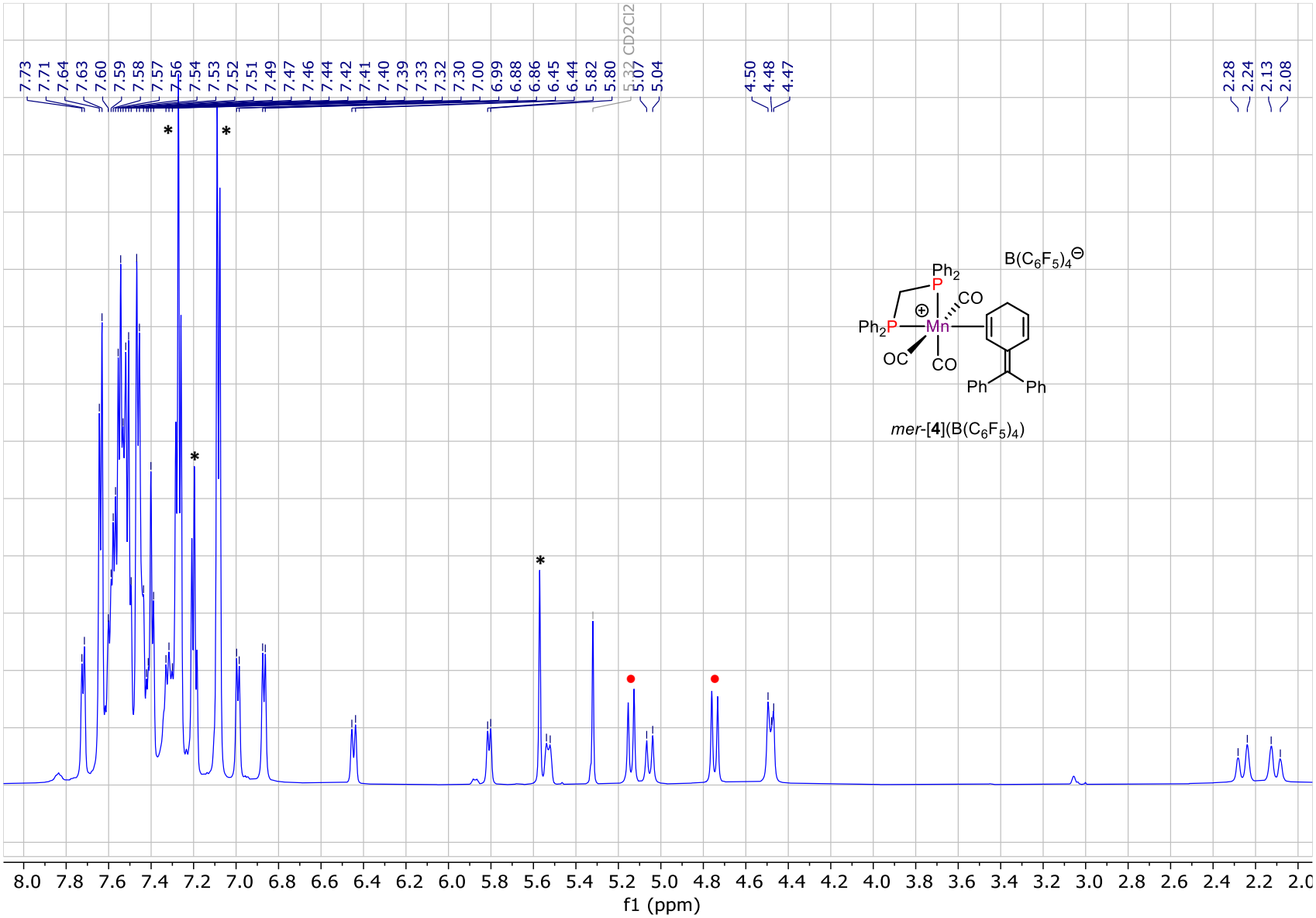

Figure S21. Section of $^{1}H\{^{31}P\}$ NMR spectrum of the reaction between complex *fac*-**1** and $[Ph_3C](B(C_6F_5)_4)$ (600.1 MHz, CD_2Cl_2, 183 K), only the signals of *mer*-[**4**]$(B(C_6F_5)_4)$ are identified. The signals of non-coordinated Ph_3CH are marked with asterisk, and those of *fac*-[**3**]$(B(C_6F_5)_4)$ with red dots.

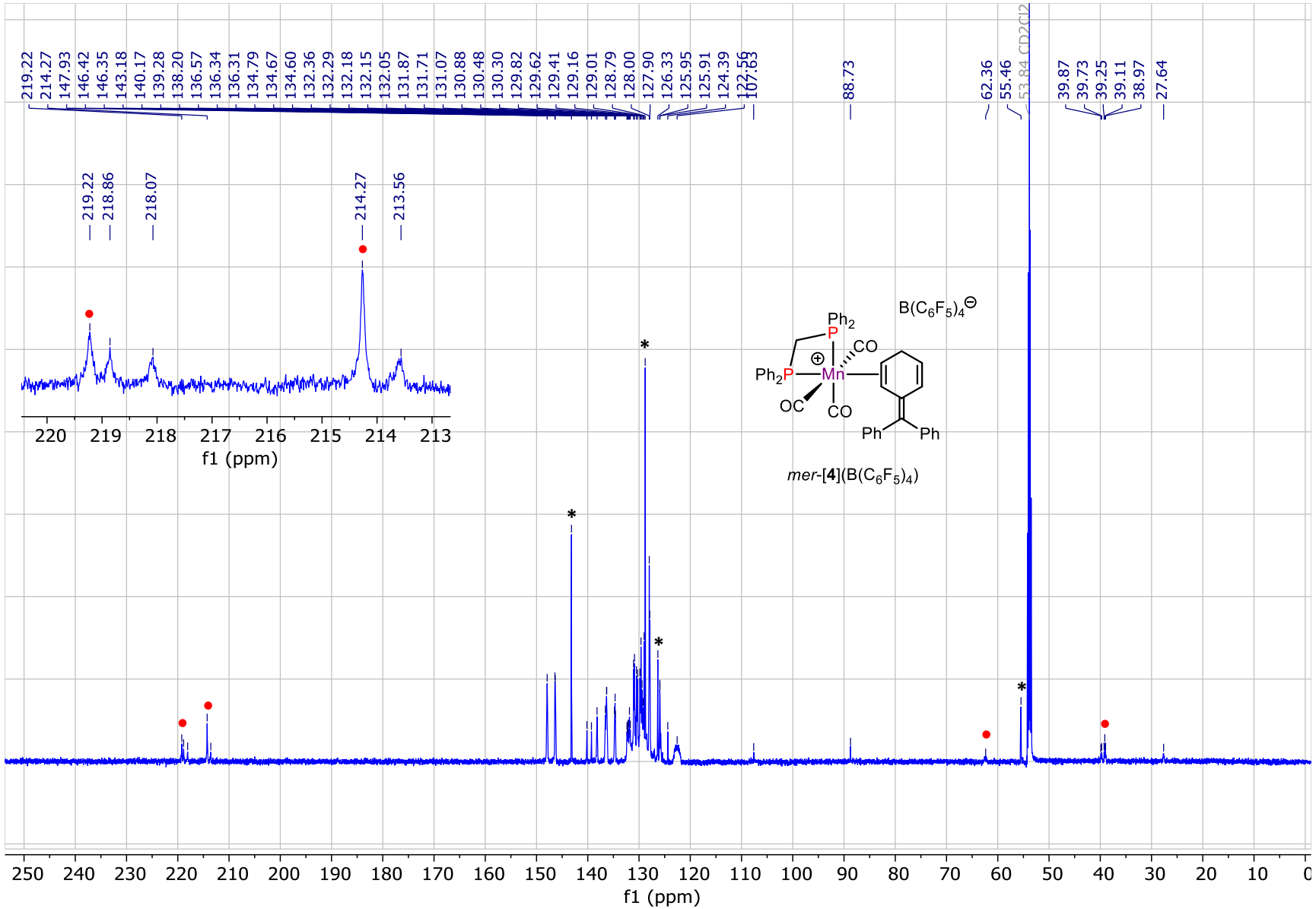

Figure S22. $^{13}C\{^{1}H\}$ NMR spectrum of mixture of *mer*-[**4**]($B(C_6F_5)_4$) and *fac*-[**3**]($B(C_6F_5)_4$) at 183 K (150.9 MHz, CD_2Cl_2, 183 K), the signals of triphenylmethane are marked with asterisk, and those of *fac*-[**3**]($B(C_6F_5)_4$) with red dots.

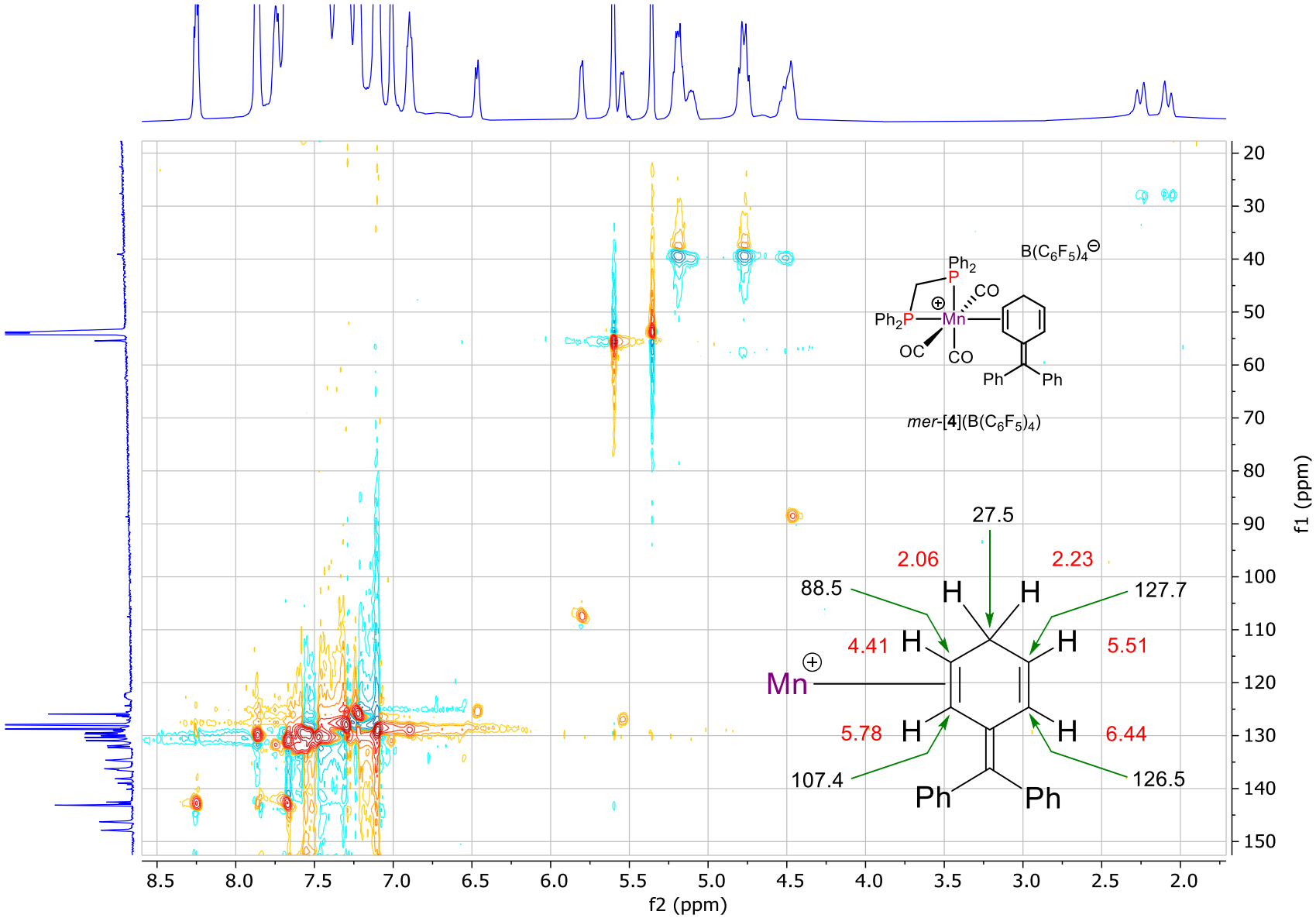

Figure S23. $^{13}C–^{1}H$ HSQC NMR spectrum for the mixture of *mer*-[**4**]($B(C_6F_5)_4$) and *fac*-[**3**]($B(C_6F_5)_4$) at 183 K (150.9 MHz, CD_2Cl_2, 183 K, cross-peaks for CH an CH_2 fragments are shown in red and blue, respectively) and correlation scheme in 1,4-cyclohexadiene moiety.

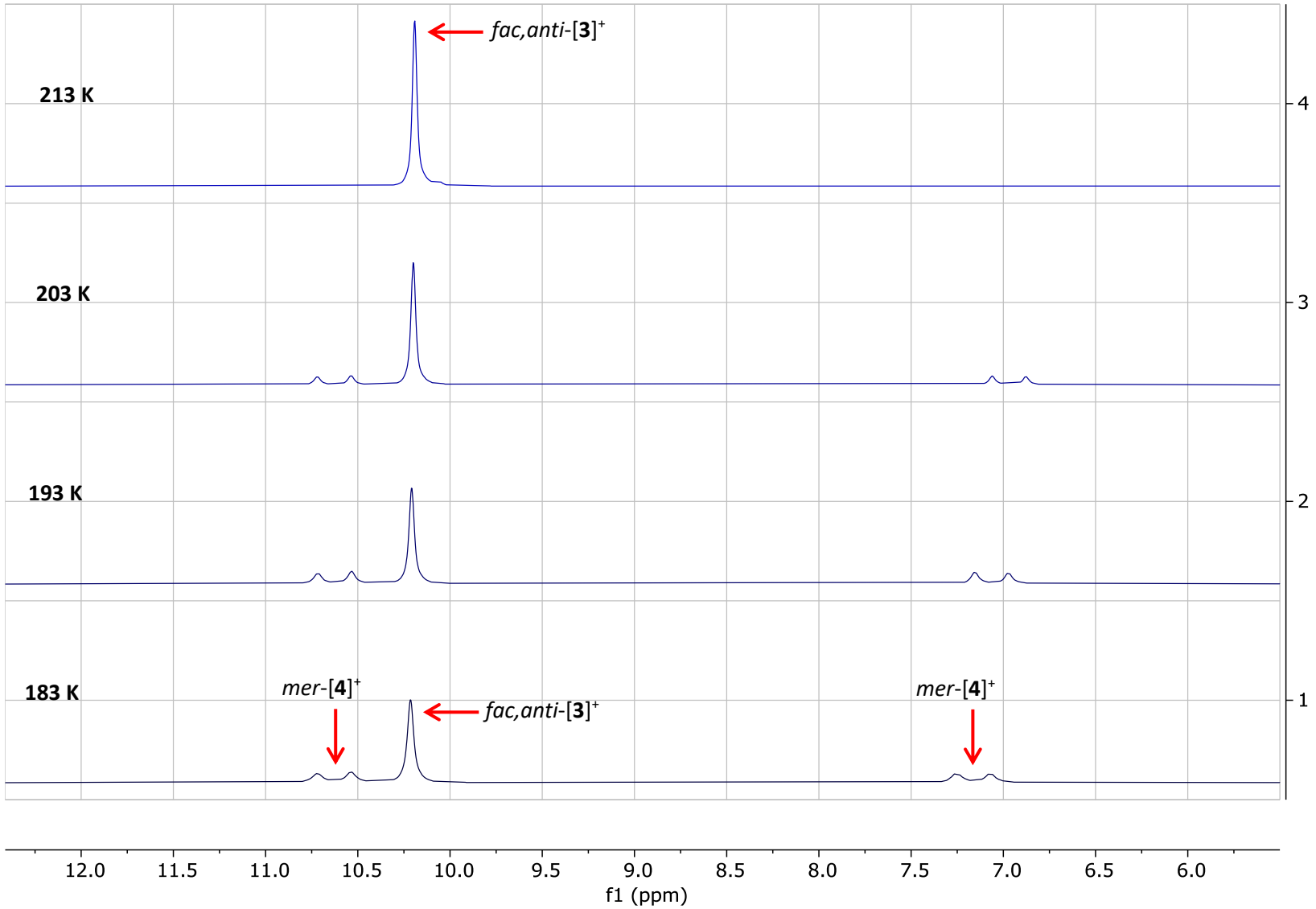

Figure S24. $^{31}P\{^{1}H\}$ NMR monitoring of the reaction between *fac*-**1** and $[Ph_3C](B(C_6F_5)_4)$ in 183-213 K temperature range (243 MHz, CD_2Cl_2).

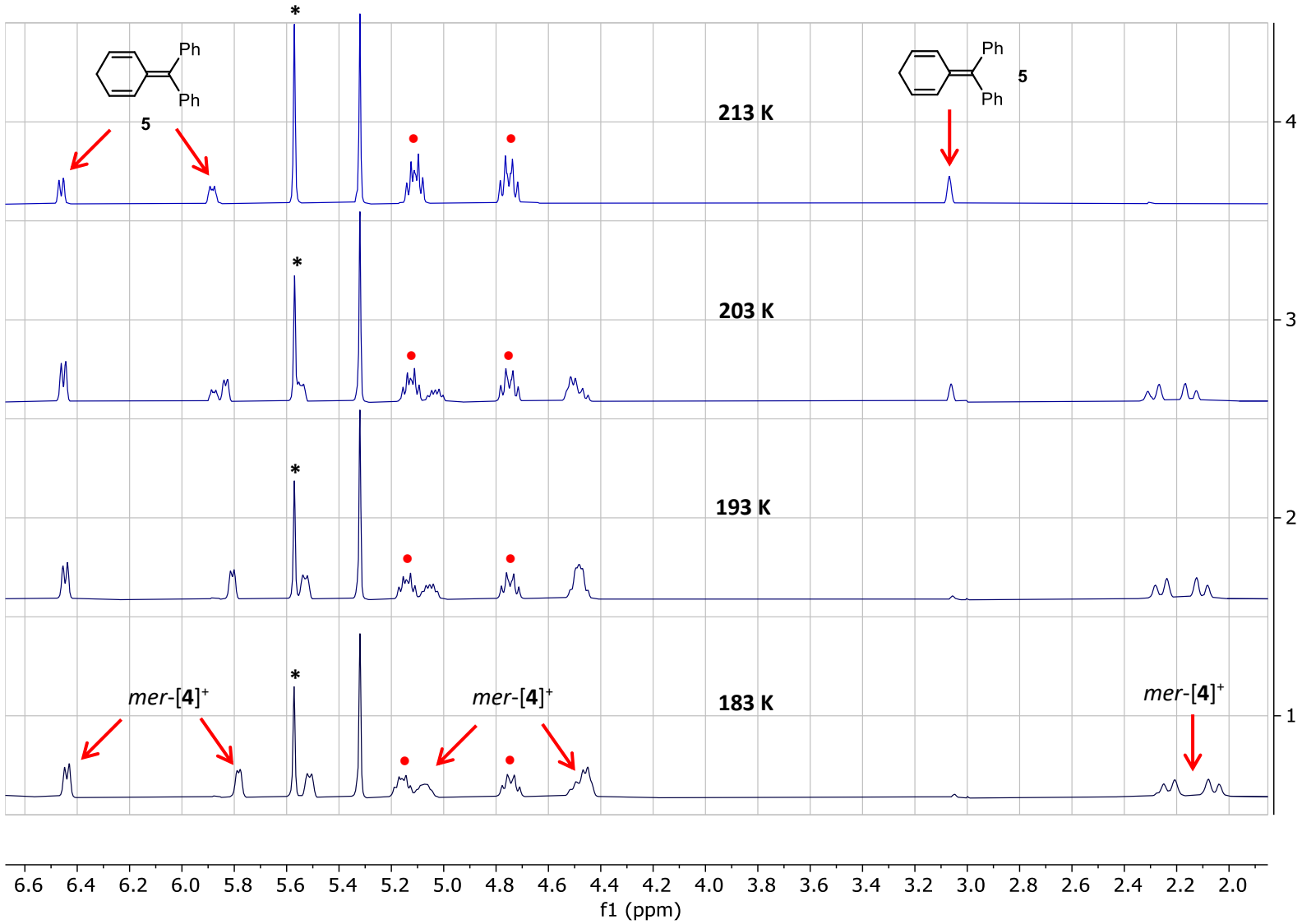

Figure S25. Section of ^{1}H NMR spectra (600.1 MHz, CD_2Cl_2) in 183-213 K temperature range illustrating the transformation of *mer*-[**4**]($B(C_6F_5)_4$) into *fac*-[**3**]($B(C_6F_5)_4$) and cyclic diene **5**, the signals of triphenylmethane are marked with asterisk, and those of *fac*-[**3**]($B(C_6F_5)_4$) are marked with red dots.

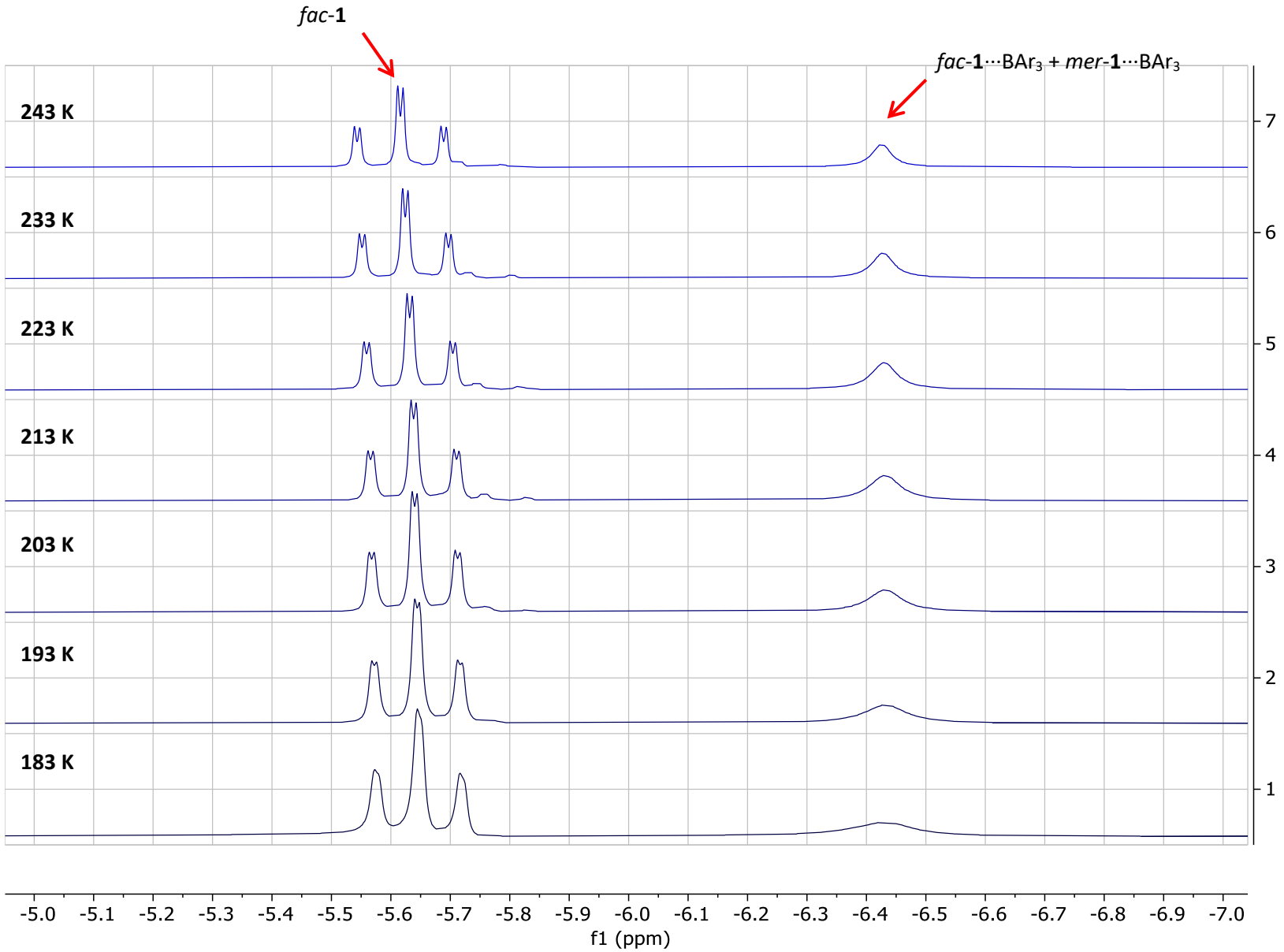

Figure S26. ^{1}H NMR monitoring of the reaction between *fac*-**1** and $B(C_6F_5)_3$ in 183-243 K temperature range in hydride signals region (600.1 MHz, CD_2Cl_2).

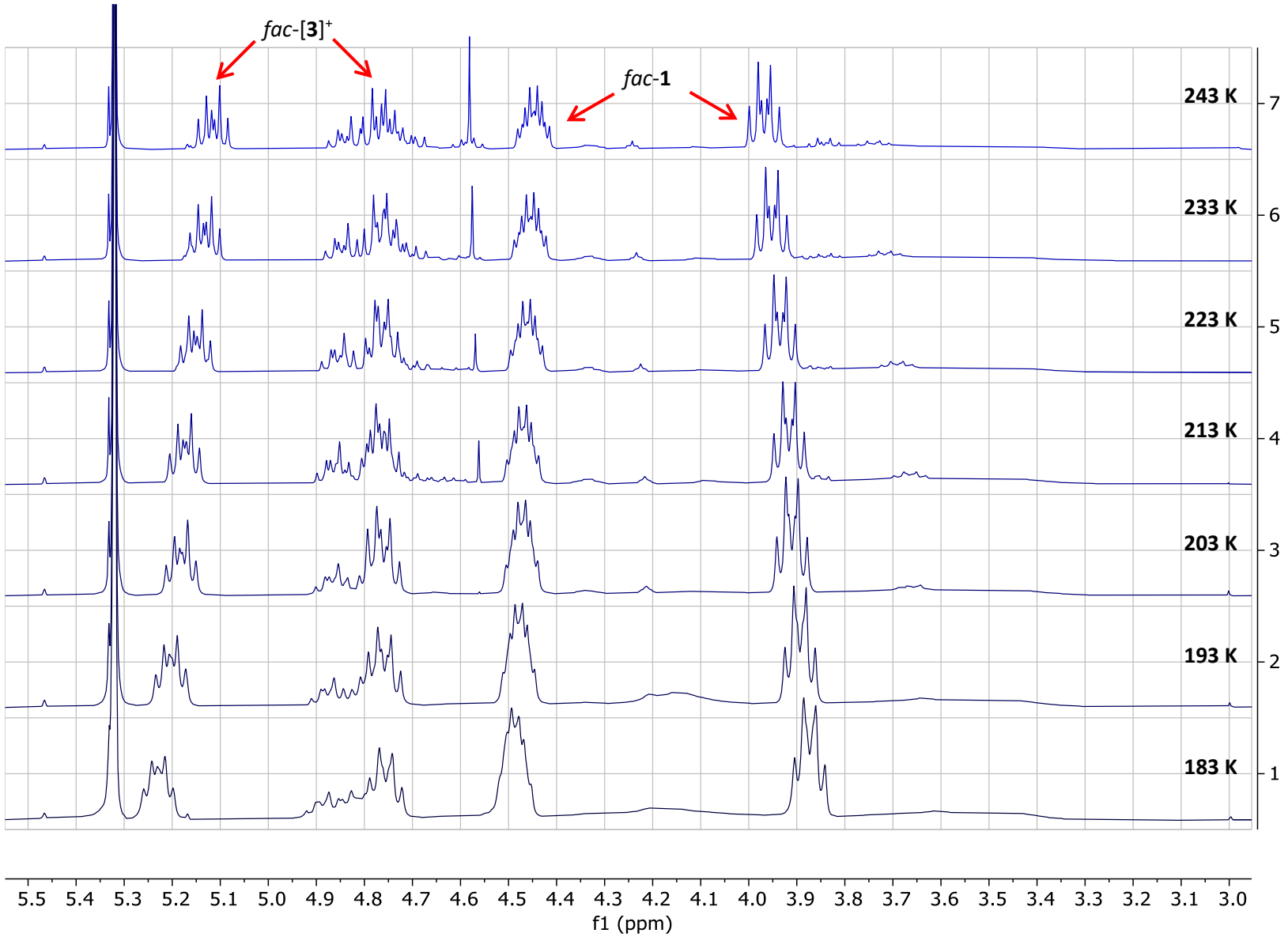

Figure S27. ^{1}H NMR monitoring of the reaction between *fac*-**1** and $B(C_6F_5)_3$ in 183-243 K temperature range in PCH_2P signals region (600.1 MHz, CD_2Cl_2).

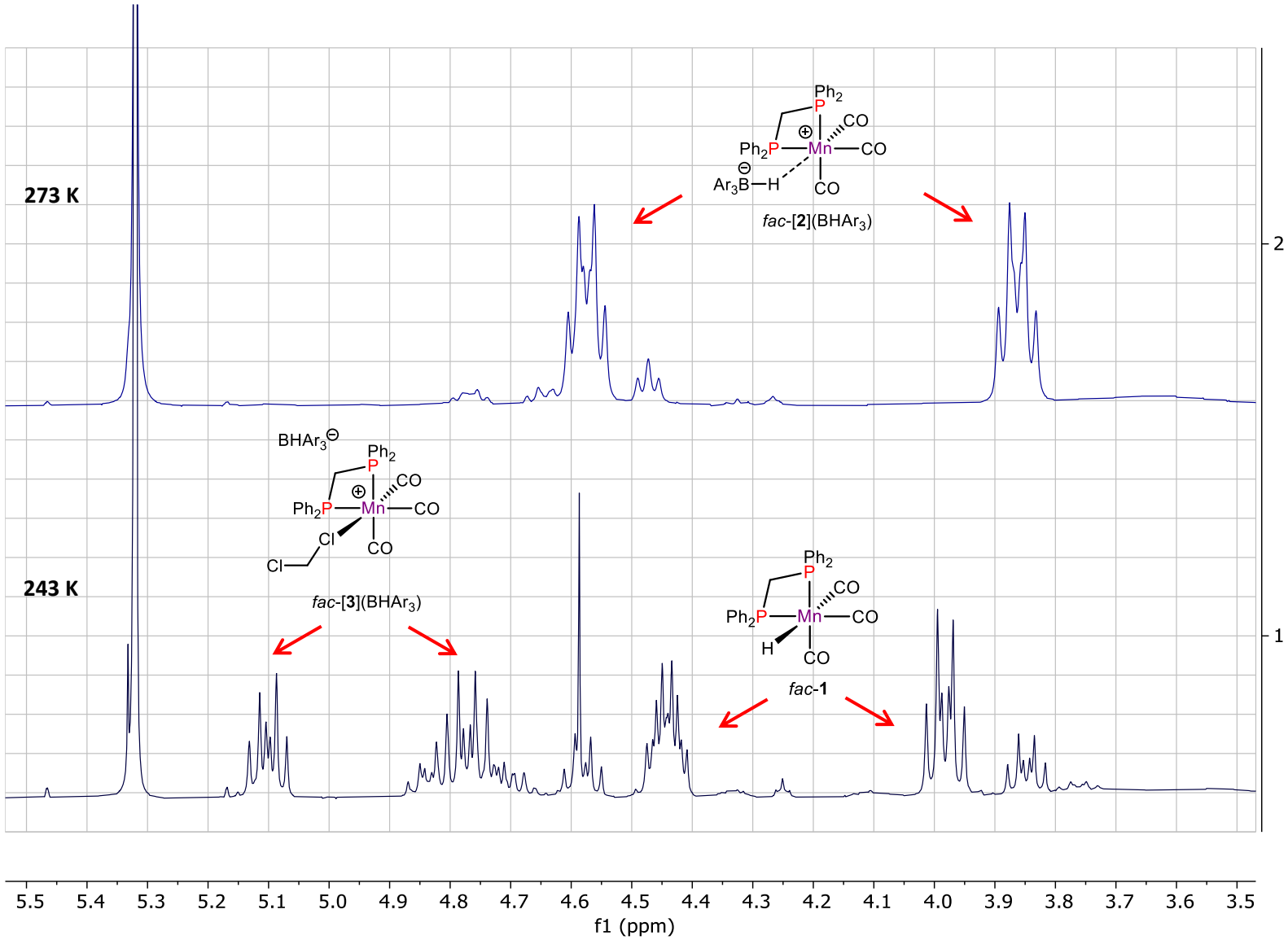

Figure S28. Superposition of ^{1}H NMR spectra of the reaction between *fac*-**1** and $B(C_6F_5)_3$ at 243 and 273 K in PCH_2P signals region illustrating the transformation of *fac*-[**3**]($BHPh_3$) into *fac*-[**2**]($BHPh_3$) (600.1 MHz, CD_2Cl_2).

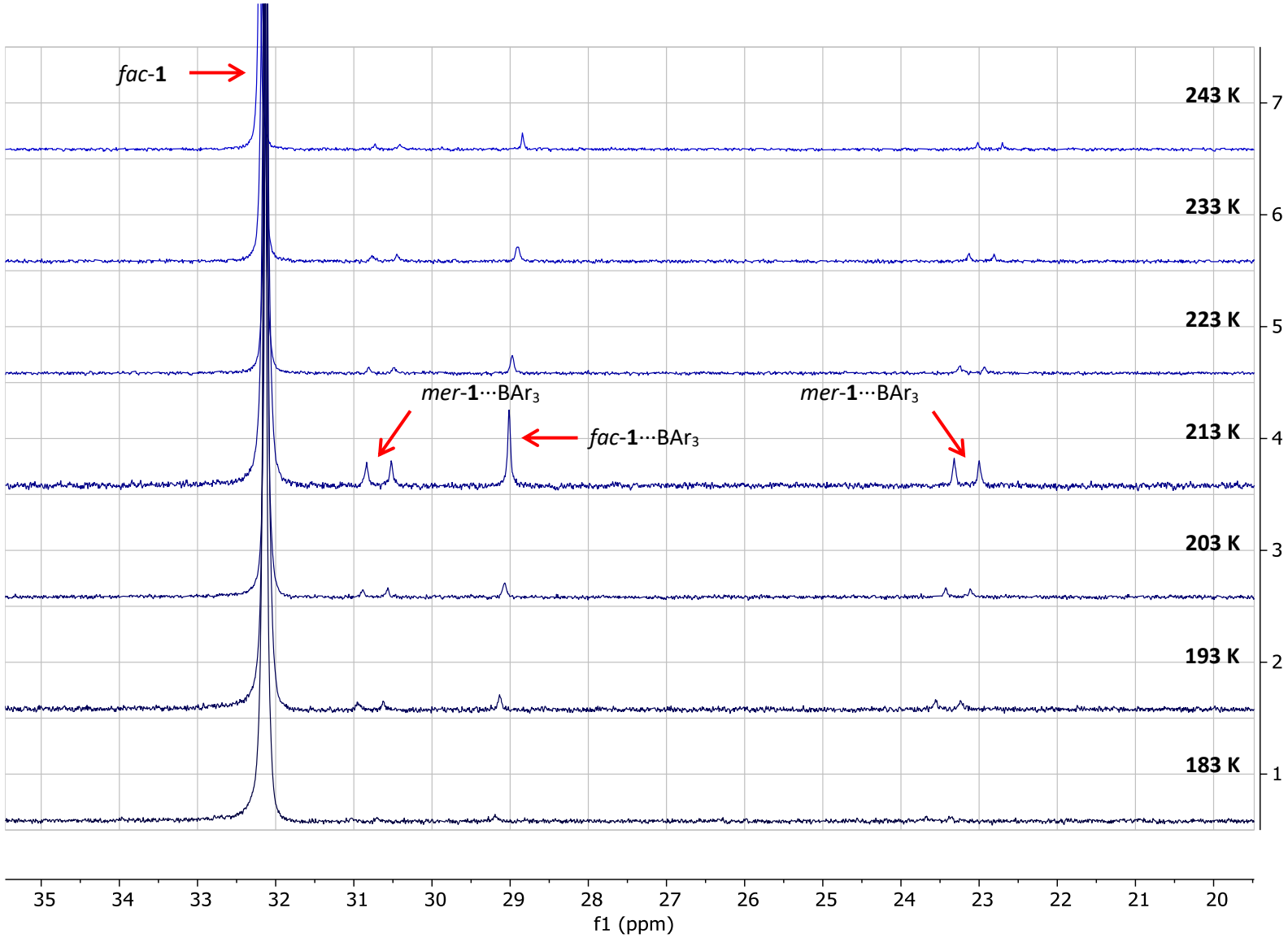

Figure S29. Section of $^{31}P\{^{1}H\}$ NMR spectra of the reaction between *fac*-**1** and $B(C_6F_5)_3$ in 183-243 K temperature range illustrating the formation of non-covalent adducts *fac*-**1**···BAr_3 and *mer*-**1**···BAr_3.

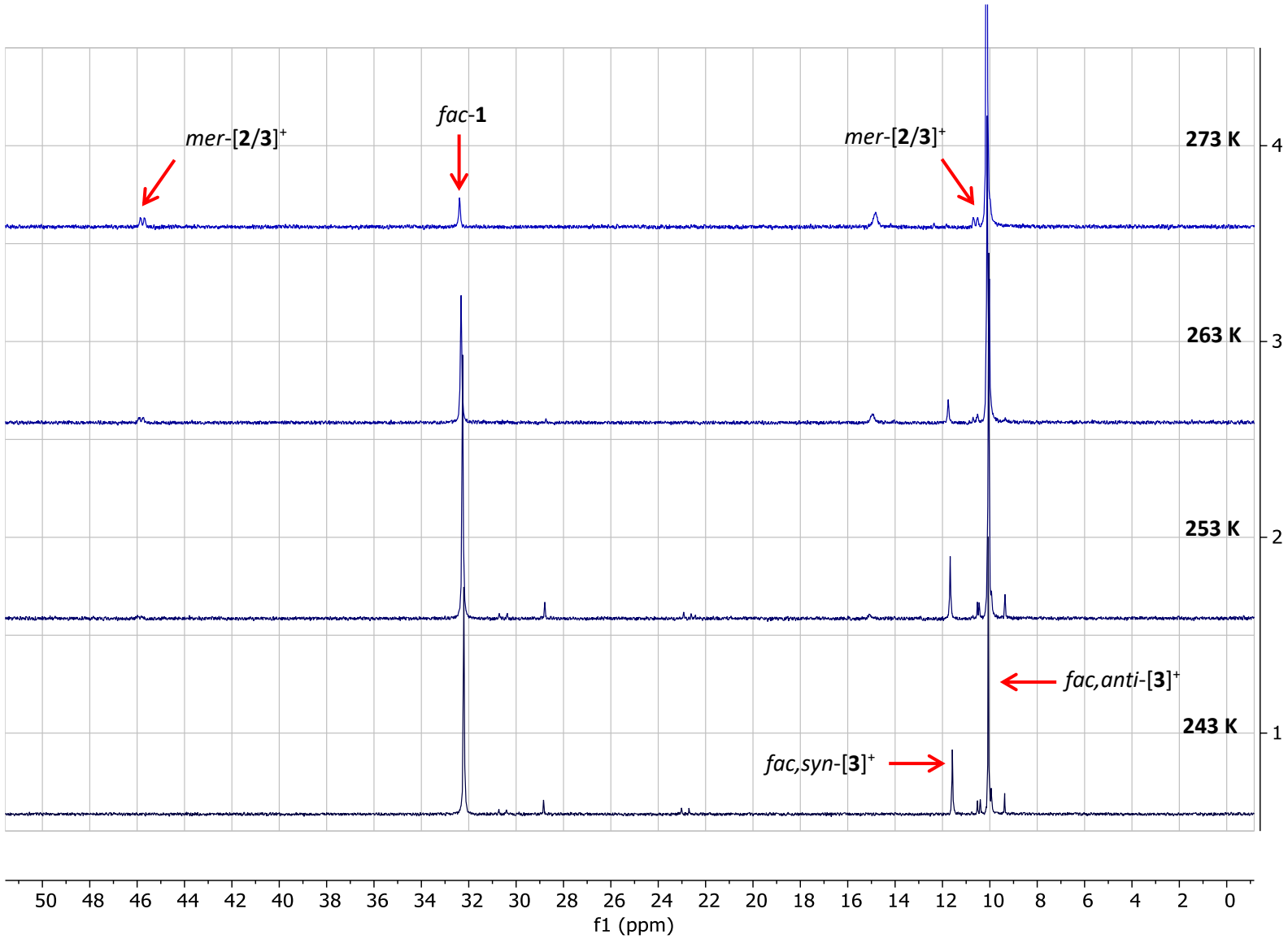

Figure S30. Section of $^{31}P\{^{1}H\}$ NMR spectra of the reaction between *fac*-**1** and $B(C_6F_5)_3$ in 243-273 K temperature range illustrating the formation of meridional cationic species *mer*-[**3**]($BHAr_3$) and/or *mer*-[**2**]($BHAr_3$).

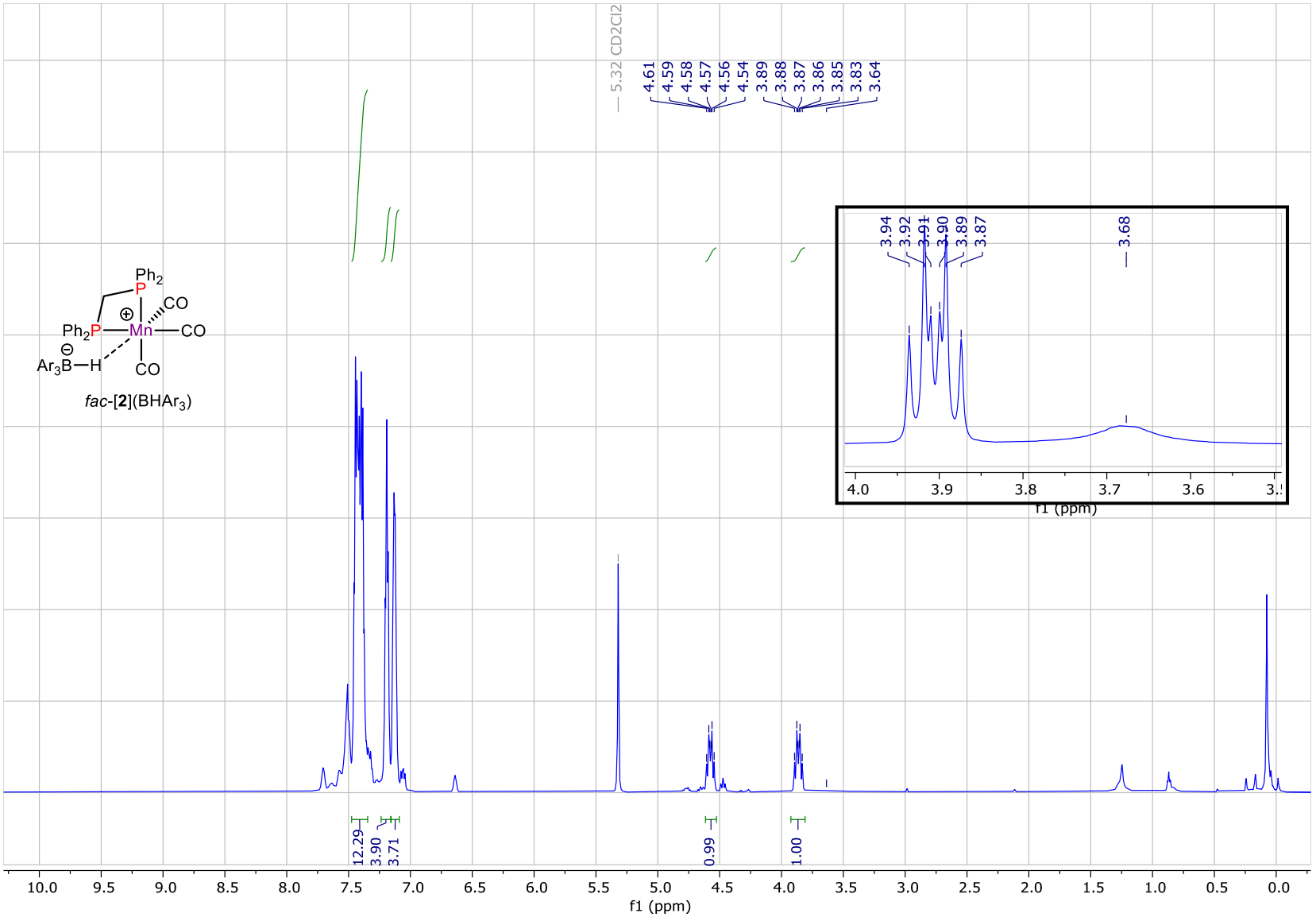

fac-[**2**](BHAr$_3$)

Figure S31. ^{1}H NMR spectrum of complex *fac*-[**2**](BHAr$_3$) (600.1 MHz, CD_2Cl_2, 273 K), inset correspond to the section of ^{1}H{^{11}B} NMR spectrum evidencing broad signal of the B–H moiety coordinated to the metal atom.

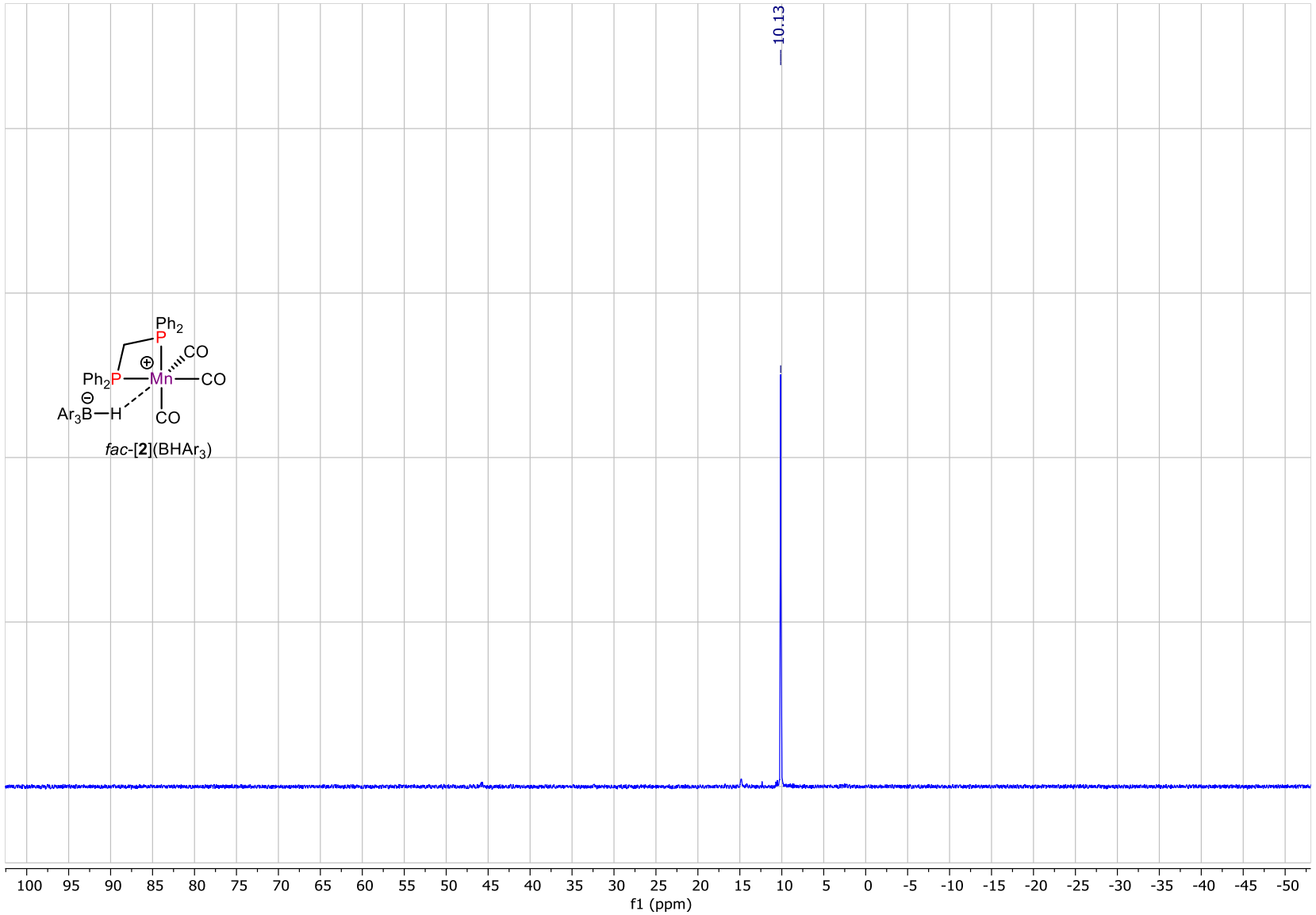

Figure S32. $^{31}P\{^{1}H\}$ NMR spectrum of complex *fac*-[**2**](BHAr$_3$) (243.0 MHz, CD_2Cl_2, 273 K).

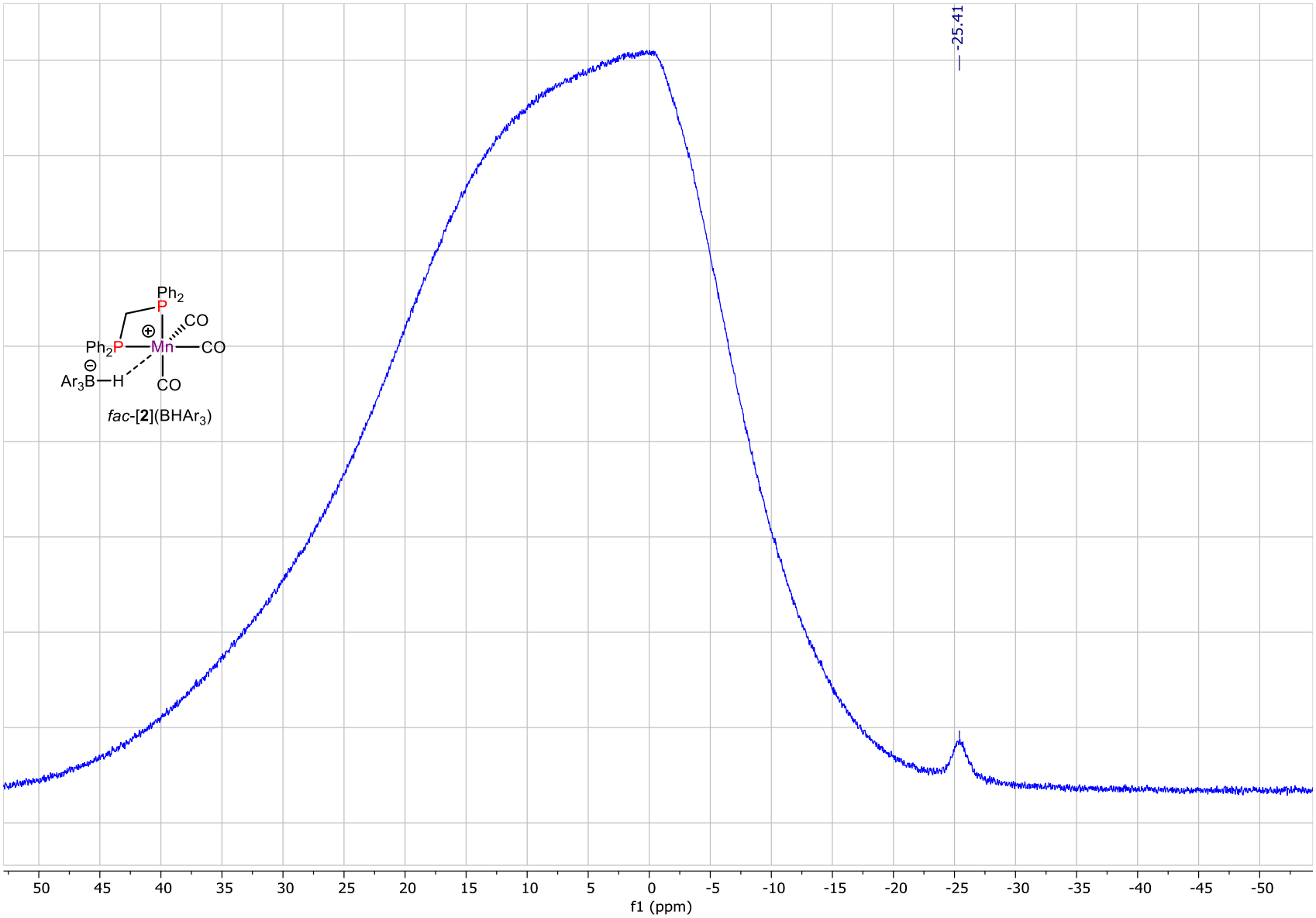

Figure S33. ^{11}B NMR spectrum of complex *fac*-[**2**](BHAr$_3$) (192.5 MHz, CD_2Cl_2, 273 K).

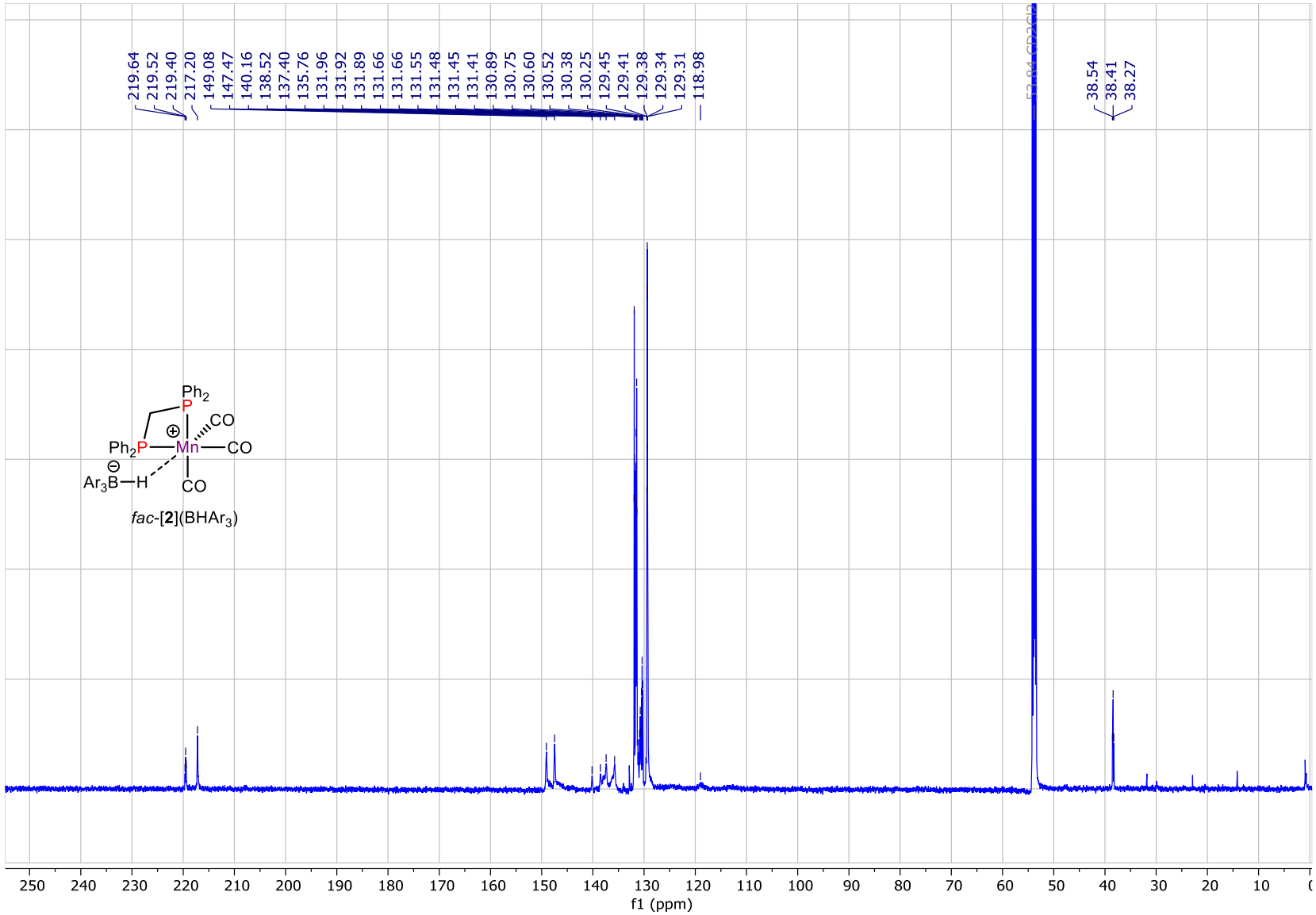

Figure S34. $^{13}C\{^{1}H\}$ NMR spectrum of complex *fac*-[**2**](BHAr$_3$) (150.9 MHz, CD_2Cl_2, 253 K).

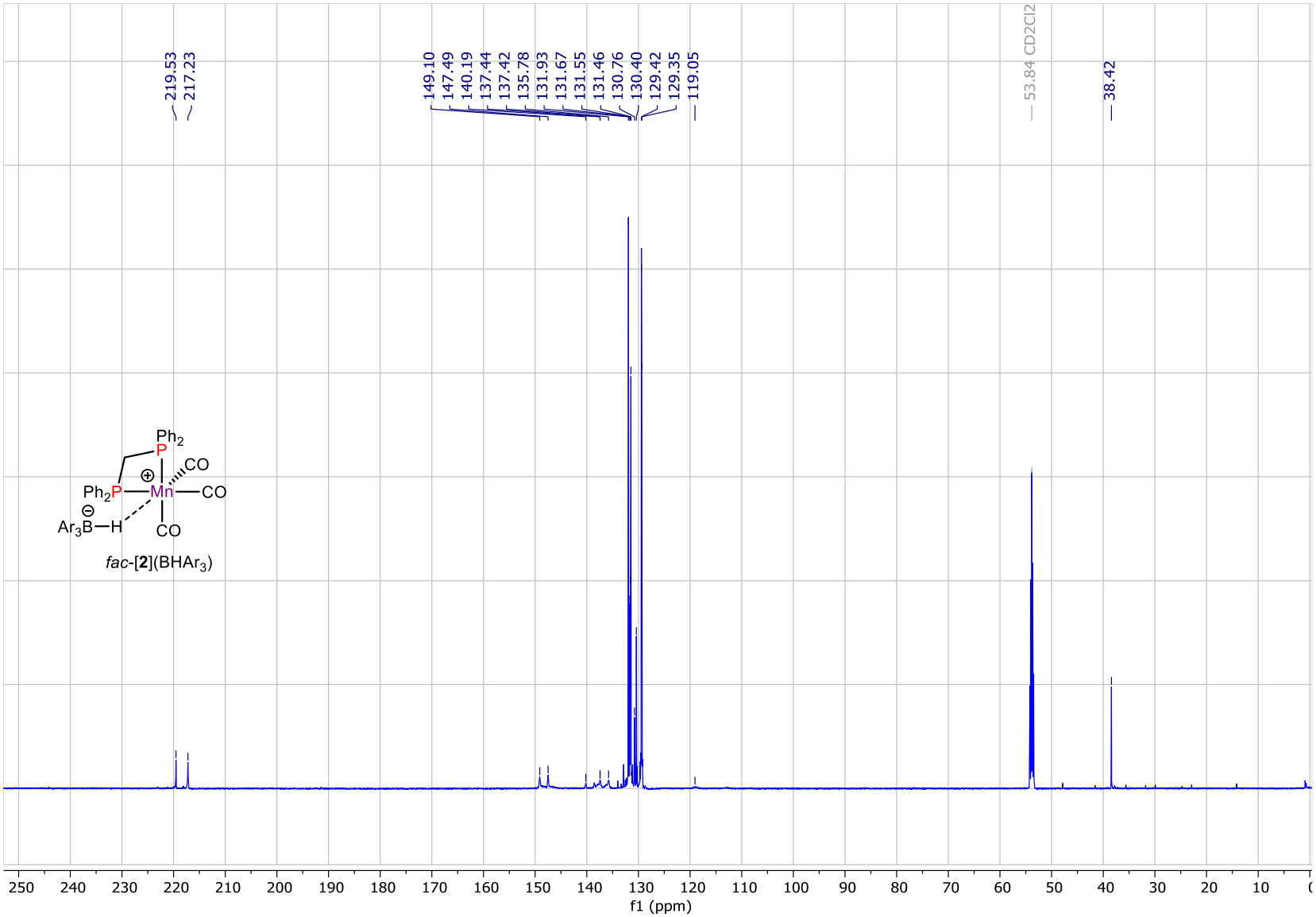

Figure S35. $^{13}C\{^{1}H,^{31}P\}$ NMR spectrum of complex *fac*-[**2**](BHAr$_3$) (150.9 MHz, CD_2Cl_2, 253 K).

DFT calculations.

Structures of reactants and complexes were optimized at the ωB97-XD level[4] applying def2-TZVP basis set[5] by Gaussian 09.[6] Optimizations were done in CH_2Cl_2 introduced by SMD solvent model.[7] Infrared frequencies were scaled by a factor 0.950.[8] Manganese hydride complex (dppm)Mn(CO)$_3$H (**1**) has two minima on PES having facial and meridional arrangement of three carbonyl groups (Figure S36). At that *fac*-**1** has *syn*-arrangement of CH_2-bridge of dppm-ligand respective to the hydride ligand, the minima corresponding to the *anti-fac*-**1** isomer was not revealed.

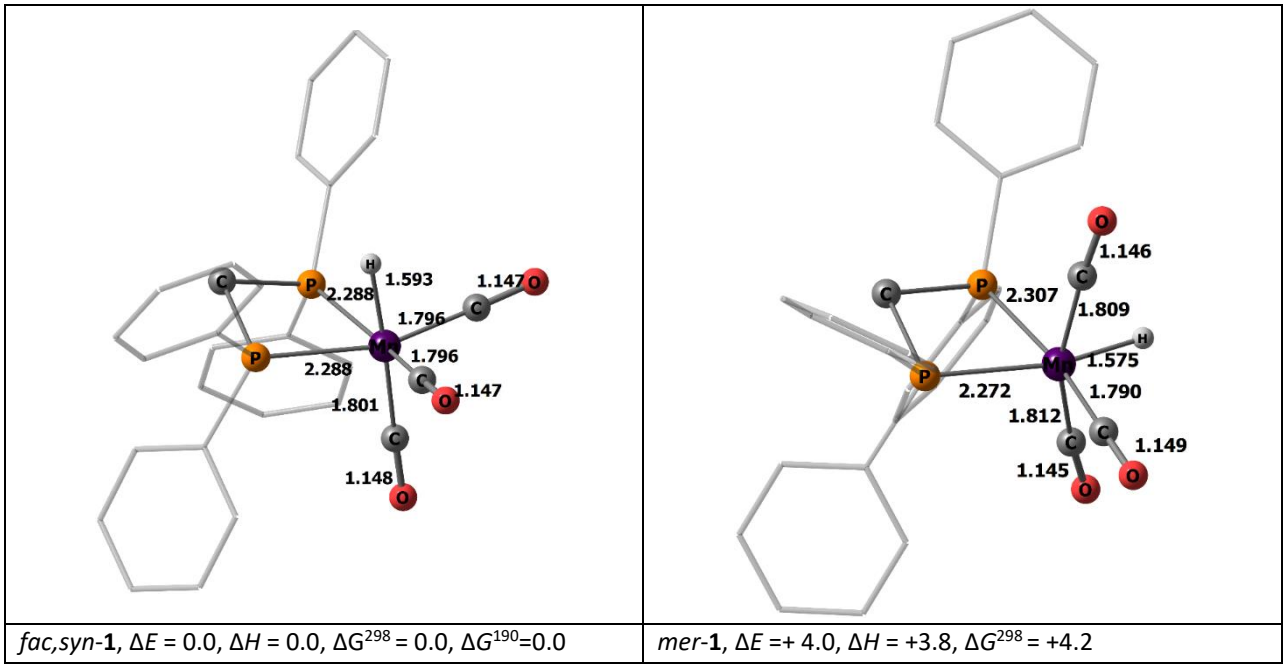

fac,syn-**1**, ΔE = 0.0, ΔH = 0.0, ΔG^{298} = 0.0, ΔG^{190}=0.0	*mer*-**1**, ΔE =+ 4.0, ΔH = +3.8, ΔG^{298} = +4.2

Figure S36. Optimized structures of two isomers for Mn(I) hydride complex (dppm)Mn(CO)$_3$H (**1**). Hydrogen atoms except hydride are removed for clarity and phenyl rings are shown as a wireframe. Energies in kcal/mol are relative to *fac*-**1**.

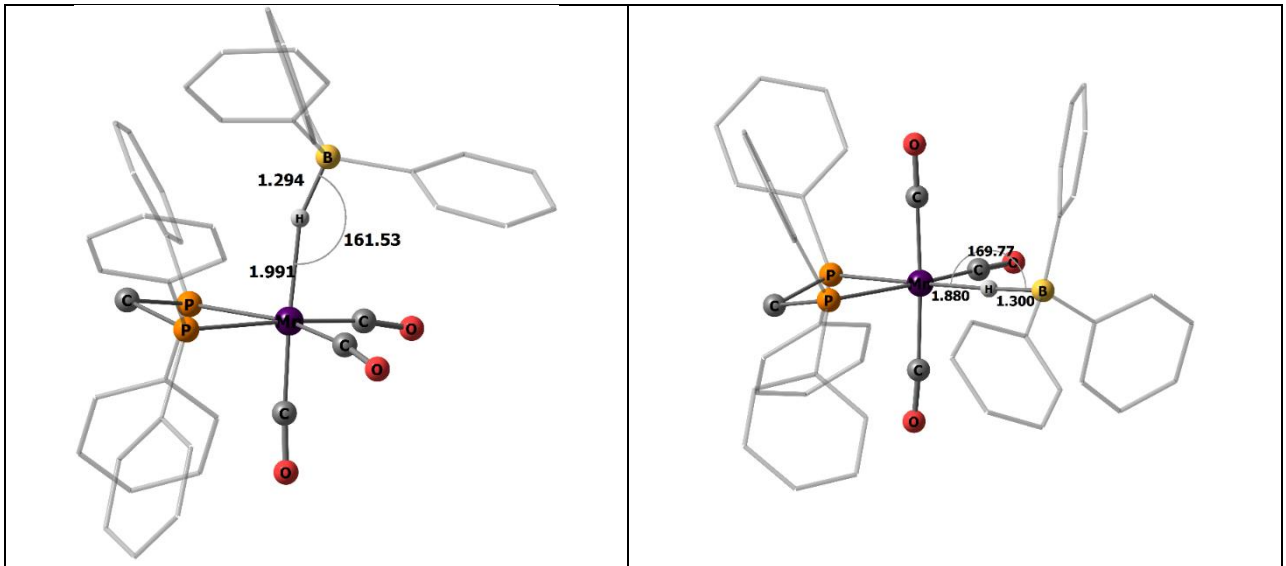

fac-**1**···BAr$_3$: ΔE=-20.1, ΔH=-18.2, ΔG^{298}=+0.2, ΔG^{190}=−6.5	*mer*-**1**···BAr$_3$: ΔE=-20.7, ΔH=-18.9, ΔG^{298}=-0.7, ΔG^{190}=−7.4

Figure S37. Optimized structures of the possible isomers of **1**···BAr$_3$ complexes. Hydrogens (except hydride) and fluorine removed, phenyl carbons shown as a wireframe. Energies in kcal/mol are relative to *fac*-**1** and free BAr$_3$.

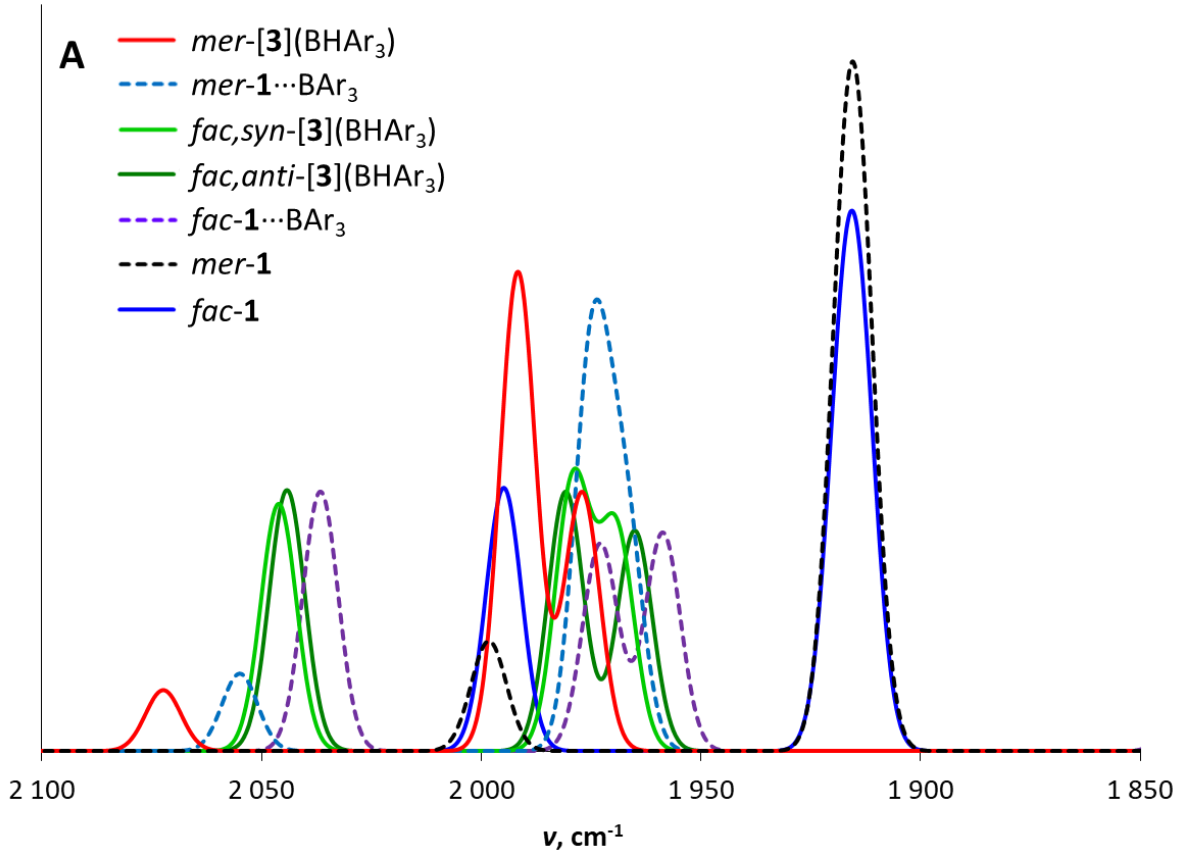

Figure S38. Simulated IR spectra for isomers of hydride **1**, their adducts with BAr_3 and cations [**3**]($BHAr_3$). Frequencies scales by 0.950, FWHH set to 9.5.

The frequency analysis for **1**, **3** and [*mer*-**1**]···BAr_3 adducts shows that vibrations which are higher than *ν*(CO) of facial cation **3** is unambiguously belongs to the meridional isomers.

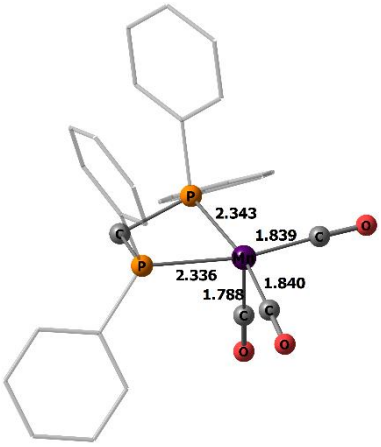	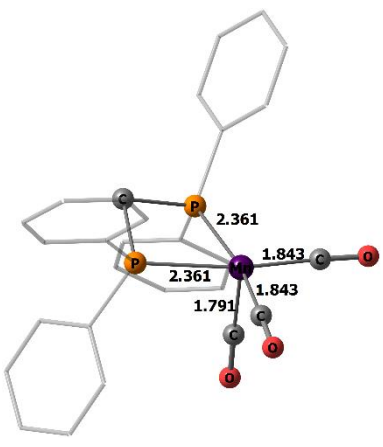	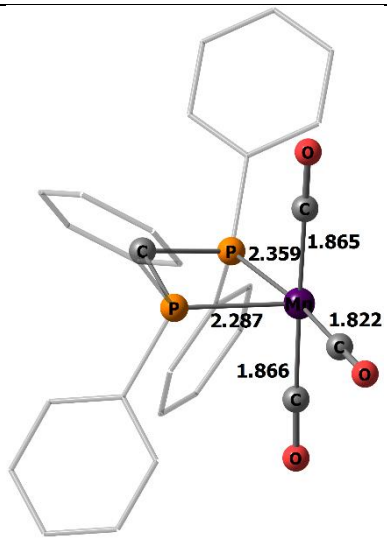
fac,anti-[**2**]$^+$ ΔE = 0.0, ΔH = 0.0, ΔG^{298} = 0.0	*fac,syn*-[**2**]$^+$ ΔE = +3.4, ΔH = +3.3, ΔG^{298} = +3.4	*mer*-[**2**]$^+$ ΔE = +6.6, ΔH = +6.5, ΔG^{298} = +6.3

Figure S39. Optimized structures of non-stabilized [(dppm)$Mn(CO)_3$]$^+$ cations [**2**]$^+$ with key geometric parameters. Hydrogens are removed, phenyl carbons shown as a wireframe. Energies in kcal/mol are relative to most stable *fac,anti*-**2**$^+$.

The *fac,anti*-[**3**]$^+$ and *fac,syn*-[**2**]$^+$ cations retain C_s symmetry of the parent facial hydride (Mn-P distances differs by <0.01 Å), while difference of Mn−P bonds is 0.072 Å for *mer*-[**2**]$^+$ isomer. Due to non-planarity of MnPCP cycle two "apical" CO groups becomes non-equivalent.

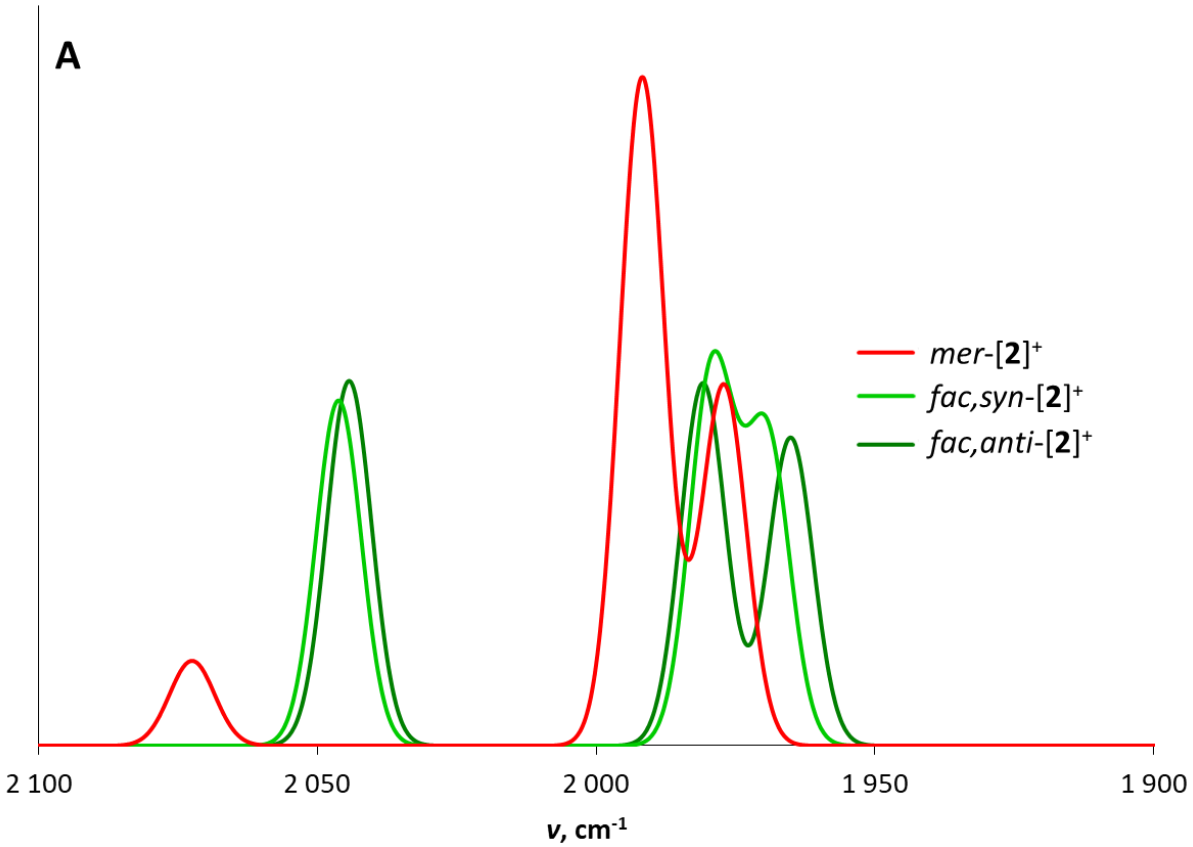

Figure S40. Simulated IR spectra for isomers of complex [(dppm)Mn(CO)$_3$]$^+$ [**2**]$^+$. Frequencies scales by 0.950, FWHH set to 9.5.

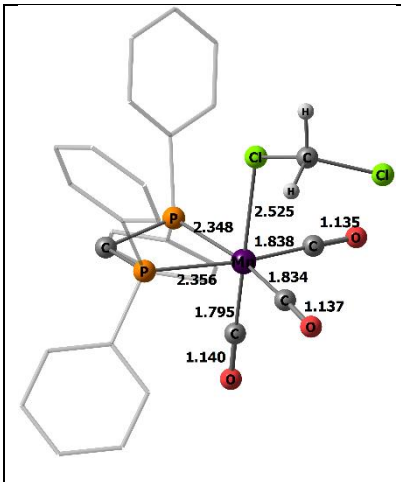	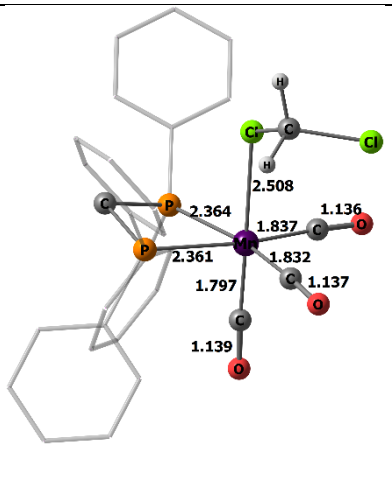	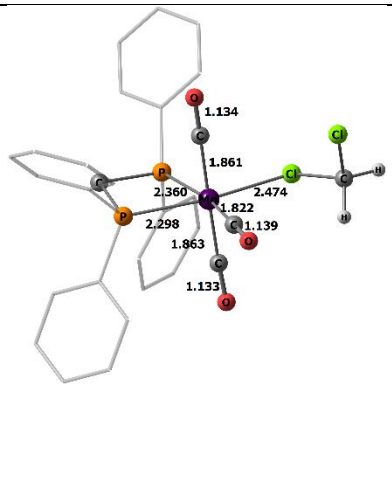
fac,anti-[**3**]$^+$ ΔE = 0.0, ΔH = 0.0, ΔG^{298} = 0.0	*fac,syn*-[**3**]$^+$ ΔE = +0.2, ΔH = +0.1, ΔG^{298} = −0.5	*mer*-[**3**]$^+$ ΔE = +2.5, ΔH = +2.4, ΔG^{298} = +2.4

Figure S41. Optimized structures of *fac*-[(dppm)Mn(CO)$_3$(κ^1*Cl*-CH_2Cl_2)](BAr$_4$) ([**3**]$^+$) with key geometric parameters. Hydrogens except those of CH_2Cl_2 are removed, phenyl carbons are shown as a wireframe. Energies in kcal/mol are relative to the *fac,anti*-[**3**]$^+$ isomer.

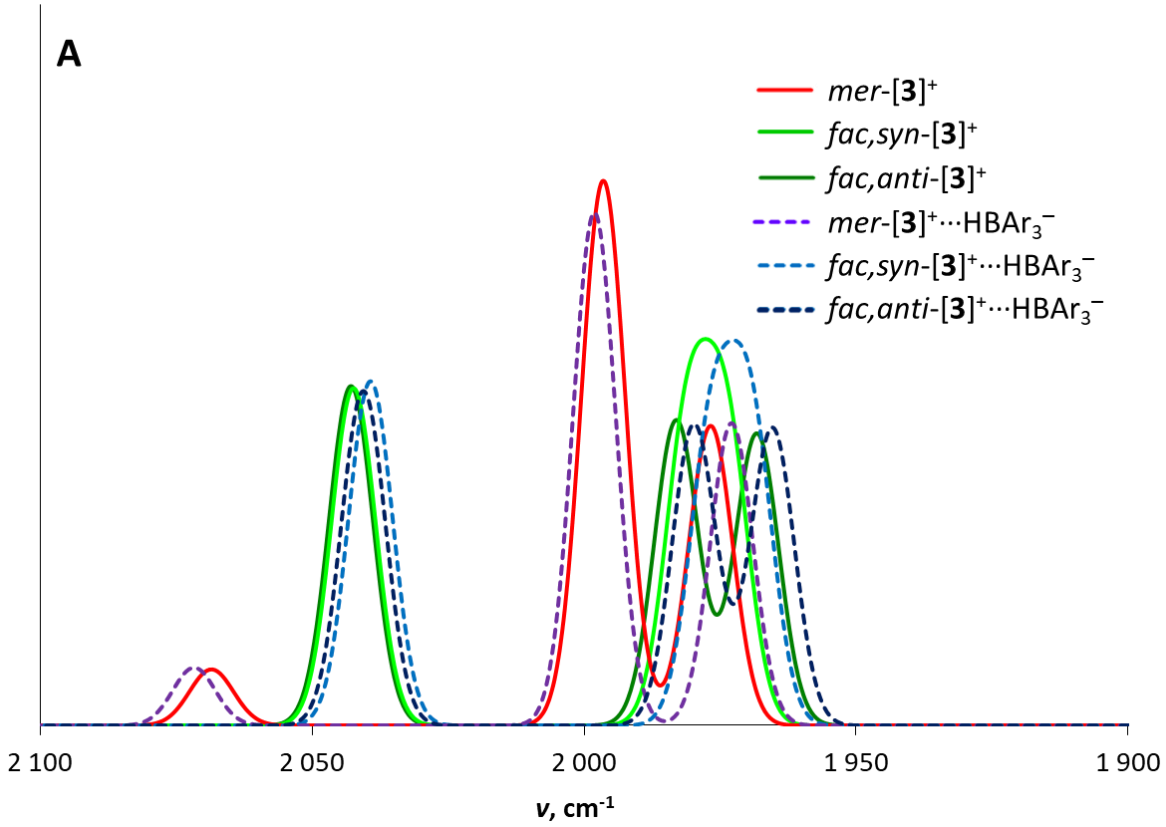

Figure S42. Comparison of simulated IR spectra for cationic complexes with coordinated CH_2Cl_2 [**3**]$^+$ *vs.* their ion pairs [**3**]($BHAr_3$). Frequencies scales by 0.950, FWHH set to 9.5.

Specific CH_2Cl_2 solvatation significantly changes the energetic pattern of cationic complexes. The most favored isomer at this conditions being the *fac,syn*-one (in the Gibbs energy scale). Notably the relative preference of *syn*- and *anti*-isomers are clearly depending on the coordination of Mn atom – if covalent bond is formed – in hydride or bromide – only *syn*-form could be found, when the coordination site is fully opened – in the free cation – the *anti*-isomer is strongly preferred. CH_2Cl_2 complexes occupy the intermediate position in this row and in this case *fac,syn*- and *fac,anti*-isomers become almost isoergic.

Another notable result is a unfavorable character of *fac,anti*-[(dppm)$Mn(CO)_3$(κ^1*Cl*-CH_2Cl_2)](BAr_4) (*fac,anti*-[**3**]$^+$) complex formation in the Gibbs energy scale, even at 190 K. It should be noted that ΔG=+2 ÷ +3 kcal/mol still allow *ca*. 10% of CH_2Cl_2 complex when using CH_2Cl_2 as a solvent due to the concentration shift of the equilibrium. Therefore we could suggest that formed as a result of hydride transfer *mer*-[**2**]$^+$ cation at low temperatures readily coordinates CH_2Cl_2 molecule to form *mer*-[(dppm)$Mn(CO)_3$(κ^1*Cl*-CH_2Cl_2)](BAr_4) (*mer*-[**3**]$^+$) solvate. The isomerization to the preferred *fac,syn*-[**3**]$^+$ complex could proceeds both directly via dissociation to the free [**2**]$^+$ cation. At the higher temperatures CH_2Cl_2 complexes are tend to dissociate with the further isomerization to the thermodynamic product *fac,anti*-[**3**]$^+$.

Table S2. Energies of CH_2Cl_2 complexes formation for [**3**]$^+$ ([**2**]$^+$ + CH_2Cl_2→ [**3**]$^+$).

	fac,anti-[**3**]$^+$	*fac,syn*-[**3**]$^+$	*mer*-[**3**]$^+$
ΔE	-7.5	-10.6	-11.6
ΔH	-5.8	-9.0	-9.9
ΔG^{298}	6.8	2.9	3.0
ΔG^{190}	2.2	-1.5	-1.7

Table S3. Calculated ν_{CO} frequencies (scaled by factor 0.95) and intensities for Mn(I) complexes **1**, [**2**]$^+$ and [**3**]$^+$ and [**3**](BHAr$_3$)

Complex	(dppm)Mn(CO)$_3$H **1^H**		(dppm)Mn(CO)$_3$H···BAr$_3$ **1^H**···BAr$_3$		[(dppm)Mn(CO)$_3$]$^+$ [**2**]$^+$			[(dppm)Mn(CO)$_3$(CH$_2$Cl$_2$)]$^+$ [**3**]$^+$			[(dppm)Mn(CO)$_3$(CH$_2$Cl$_2$)]$^+$···[HBAr$_3$]$^-$ [**3**](BHAr$_3$)		
	mer-	*fac,syn-*	*mer-*	*fac,syn-*	*mer-*	*fac,syn-*	*fac,anti-*	*mer-*	*fac,syn-*	*fac,anti-*	*mer-*	*fac,syn-*	*fac,anti-*
ν_{CO1}, cm^{-1}	1914	1914	1968	1959	1978	1970	1966	1977	1974	1969	1974	1970	1966
A_{CO1}, km/mol	2215	1901	1366	1317	1560	1331	1331	1330	1276	1297	1343	1313	1322
ν_{CO2}, cm^{-1}	1918	1918	1975	1974	1992	1980	1982	1997	1982	1984	1999	1977	1980
A_{CO2}, km/mol	2338	1785	2417	1252	2889	1629	1567	2418	1308	1356	2278	1272	1338
ν_{CO3}, cm^{-1}	1999	1996	2056	2037	2073	2047	2045	2069	2043	2044	2072	2040	2041
A_{CO3}, km/mol	664	1588	467	1566	368	1495	1576	249	1498	1509	257	1527	1487

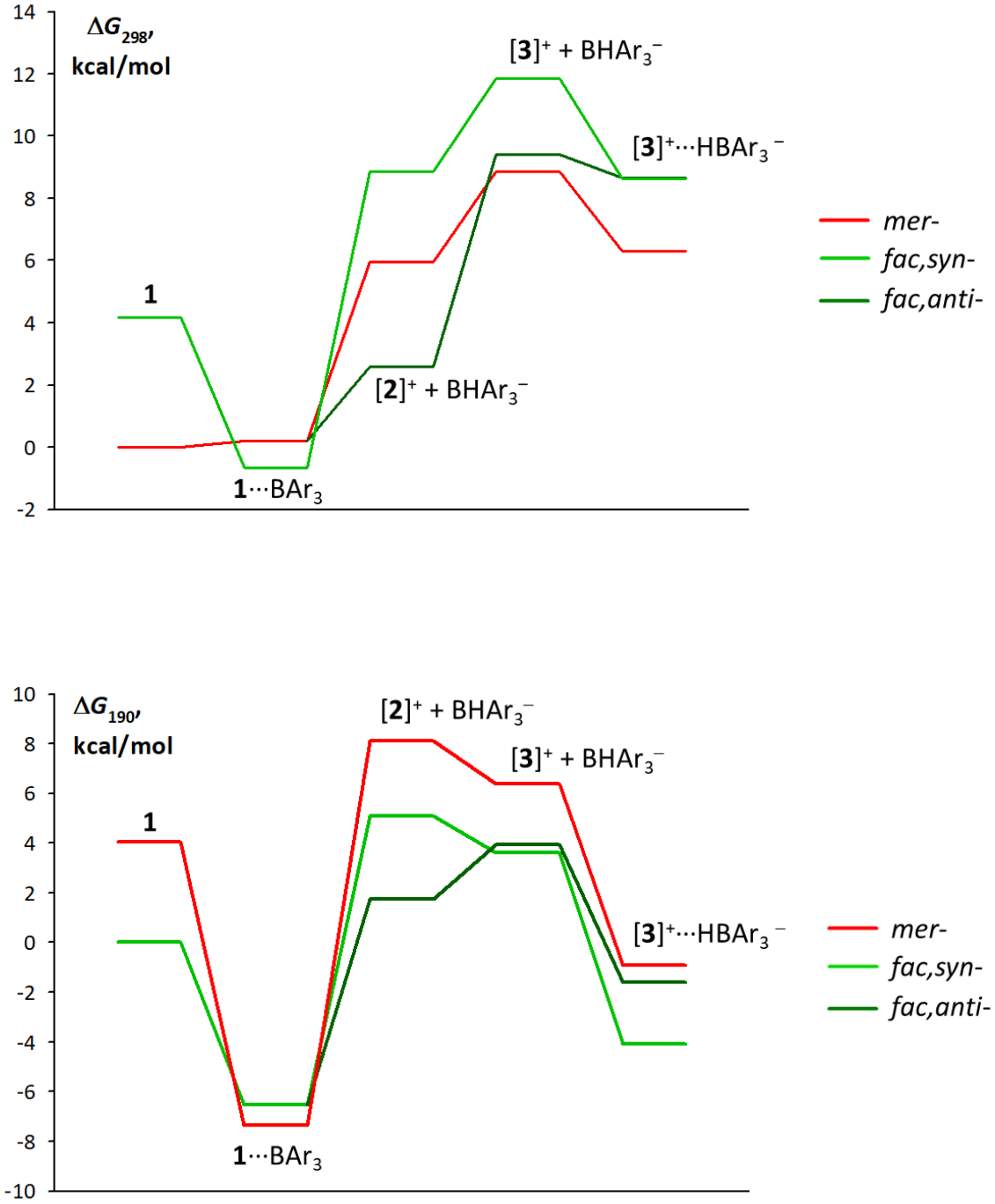

Figure S43. Computed (DFT/ωB97XD/def2-TZVP/SMD(CH_2Cl_2)) Gibbs energy profiles for the *fac*-**1** and BAr_3 reaction at 298 K (top) and 190 K (bottom).

References

1. N. V. Kireev, O. A. Filippov, E. S. Gulyaeva, E. S. Shubina, L. Vendier, Y. Canac, J.-B. Sortais, N. Lugan and D. A. Valyaev, *Chem. Commun.*, 2020, **56**, 2139.
2. A. Zirakzadeh, S. R. M. M. de Aguiar, B. Stöger, M. Widhalm and K. Kirchner, *ChemCatChem*, 2017, **9**, 1744.
3. G. R. Fulmer, A. J. M. Miller, N. H. Sherden, H. E. Gottlieb, A. Nudelman, B. M. Stoltz, J. E. Bercaw and K. I. Goldberg, *Organometallics*, 2010, **29**, 2176.
4. J.-D. Chai and M. Head-Gordon, *Phys. Chem. Chem. Phys*., 2008, **10**, 6615.
5. F. Weigend and R. Ahlrichs, *Phys. Chem. Chem. Phys.*, 2005, **7**, 3297.
6. Gaussian 09, Revision D.01, M. J. Frisch, G. W. Trucks, H. B. Schlegel, G. E. Scuseria, M. A. Robb, J. R. Cheeseman, G. Scalmani, V. Barone, G. A. Petersson, H. Nakatsuji, X. Li, M. Caricato, A. Marenich, J. Bloino, B. G. Janesko, R. Gomperts, B. Mennucci, H. P. Hratchian, J. V. Ortiz, A. F. Izmaylov, J. L. Sonnenberg, D. Williams-Young, F. Ding, F. Lipparini, F. Egidi, J. Goings, B. Peng, A. Petrone, T. Henderson, D. Ranasinghe, V. G. Zakrzewski, J. Gao, N. Rega, G. Zheng, W. Liang, M. Hada, M. Ehara, K. Toyota, R. Fukuda, J. Hasegawa, M. Ishida, T. Nakajima, Y. Honda, O. Kitao, H. Nakai, T. Vreven, K. Throssell, J. A. Montgomery, Jr., J. E. Peralta, F. Ogliaro, M. Bearpark, J. J. Heyd, E. Brothers, K. N. Kudin, V. N. Staroverov, T. Keith, R. Kobayashi, J. Normand, K. Raghavachari, A. Rendell, J. C. Burant, S. S. Iyengar, J. Tomasi, M. Cossi, J. M. Millam, M. Klene, C. Adamo, R. Cammi, J. W. Ochterski, R. L. Martin, K. Morokuma, O. Farkas, J. B. Foresman, and D. J. Fox, Gaussian, Inc., Wallingford CT, 2016.
7. A. V. Marenich, C. J. Cramer, D. G. Truhlar, *J. Phys. Chem. B*, 2009, **113**, 6378.
8. I. M. Alecu, J. Zheng, Y. Zhao, D. G. Truhlar, *J. Chem. Theory Comput.*, 2010, **6**, 2872-2887.